ELSEVIER

Coordination Chemistry Reviews 230 (2002) 5–27

COORDINATION CHEMISTRY REVIEWS

www.elsevier.com/locate/ccr

A DFT/TDDFT interpretation of the ground and excited states of porphyrin and porphyrazine complexes

E.J. Baerends [a,*], G. Ricciardi [b], A. Rosa [b,*], S.J.A van Gisbergen [a]

[a] *Afdeling Theoretische Chemie, Vrije Universiteit, De Boelelaan 1083, 1081 HV, Amsterdam, The Netherlands*
[b] *Dipartimento di Chimica, Università della Basilicata, Via N. Sauro 85, 85100 Potenza, Italy*

Received 2 October 2001; accepted 8 March 2002

Contents

Abstract

A comprehensive treatment is given of the electronic excitation spectra of Mg, Zn and Ni complexes of porphyrin and porphyrazine using time-dependent density functional theory (TDDFT). It is emphasized that the Kohn–Sham (KS) molecular orbital (MO) method, which is the basis for the TDDFT calculations, affords a MO interpretation of the ground state electronic structure and of the nature of the excitations. This implies that a direct connection can be made to many previous MO treatments of the title compounds. We discuss in particular, how the original explanations of the intensity distribution over the lowest excitations (the Q and B bands) in terms of a cyclic polyene model, or even a free-electron model, can be reconciled with the actual molecular and electronic structure of these compounds being much more complicated than these simple models. A fragment approach is used, building the porphyrin ring from pyrrole rings and CH or N bridges. This leads directly to a simple interpretation of the orbitals of Gouterman's four-orbital model, which are responsible for the Q and B bands. It also leads to additional occupied π-orbitals which are absent in the cyclic polyene model and which need to be invoked to understand other features of the electronic spectra such as

* Corresponding authors. Tel.: +31-20-444-7621; fax: +31-20-444-7629
E-mail addresses: baerends@chem.vu.nl (E.J. Baerends), rosa@unibas.it (A. Rosa).

PII: S0010-8545(02)00093-0

the origin of the N, L and M bands. Considerable attention is given to the intensities of the various transitions, explaining why the transitions within the so-called four-orbital model of Gouterman have large transition dipoles, why transitions from additional occupied π-orbitals have relatively small transition dipoles.

Keywords: Electron excitation spectra; Porphyrin; Orbital model

1. Introduction

The spectroscopic properties of porphyrin (P) and porphyrazine (Pz) complexes have attracted considerable experimental and theoretical interest since the middle of the century, initially because of their vital role in biological processes such as photosynthesis and respiration [1], more recently because of their potential technological applications [2–4]. Among others, the linear and nonlinear optical (NLO) properties of these systems are currently widely investigated in view of the design, synthesis and characterization of molecular materials for molecular electronics, optoelectronics and photonics [5–9].

The effects of *meso*-tetraaza substitution on the UV–vis absorption bands of porphyrins are to date well documented [4,10–14]. Porphyrazine complexes exhibit for instance a significant red shift and an intensification of the lowest energy $\pi \rightarrow \pi^*$ Q band, and a more complicated Soret band region due to additional $n \rightarrow \pi^*$ transitions introduced by azamethine groups.

The different nature of the porphyrin and porphyrazine ring reflects not only on the spectral features associated with macrocycle centred electronic transitions, but also on the metal-to-ligand charge transfer (MLCT) and ligand-to-metal charge transfer (LMCT) transitions appearing in the spectra of transition metal complexes. The different size of the coordination cavity causes indeed the metal–ligand interaction to change going from porphyrins to porphyrazines.

The origin and the intensities of the lowest absorptions of metal–porphyrins, the Q and the B bands, were successfully explained by Gouterman's four-orbital model [15–17]. Historically, the cyclic polyene model for the porphyrinic skeleton has played a large role [16,18,19] and is still often cited as providing a qualitative basis for the understanding of the weak Q and strong B band system of porphyrins. The LCAO-MO treatment that gives rise to the four-orbital model improves upon this by explicitly taking into account the structure of the porphyrin ring [17]. According to the four-orbital model, the B and Q bands can be described in terms of transitions between a pair of top filled orbitals (a_{1u} and a_{2u}) and lowest empty orbitals (the doubly degenerate e_g). The near degeneracy of the $a^1_{1u}e^1_g$ and $a^1_{2u}e^1_g$ excited configurations leads to a strong configuration interaction that results in a high-lying state corresponding to the B band, and a low-lying state corresponding to the Q band. The configuration mixing combines the transition dipoles of the individual one-electron transitions in such a way that the B band contains nearly all the intensity, while the Q band is weak. This model was also used to describe the optical spectra of porphyrazines [17]. The substitution of aza linkages for the methine bridges in the porphyrinic macrocycle breaks the accidental degeneracy of the a_{1u} and a_{2u} orbitals significantly. This diminishes interaction between the $(a_{1u})^1(e_g)^1$ and $(a_{2u})^1(e_g)^1$ configurations and removes the forbidden character of the low-energy transition. Therefore, the Q band is no longer weak in porphyrazines.

One step forward in understanding the electronic structure and electronic spectra of porphyrins and related macrocycles was made when Self-Consistent-Molecular-Orbital Pariser-Parr-Pople (SCMO-PPP) theory was applied to the porphyrin π system [14]. The pioneering SCMO-PPP-CI calculations by Weiss et al. [14] on porphyrins and related ring systems showed that the four-orbital model was justified for the lowest energy transitions (Q bands) but was less justified for the near-UV (Soret) transitions, specially in the case of porphyrazines where higher lying excited states are needed to describe the B band region.

Many subsequent theoretical studies, which in some cases covered a spectral range extending far beyond the B band region, have been mostly based on semiempirical models which require the use of adjustable parameters. A review can be found in Ref. [20,21].

The few density functional calculations [22–26] which have been reported before the advent of the time-dependent density functional theory (TDDFT) methods do not provide an accurate description of the optical spectra of these systems, because of their inability to account for the extensive configuration mixings which characterise the excited states of porphyrins and porphyrazines.

Highly correlated ab initio calculations have begun to appear quite recently and only concern free base porphin (FBP), [27–33] free base porphyrazine (FBPz), [33] magnesium porphyrin [33–35] and magnesium and zinc porphyrin and porphyrazine [33] complexes, transition metal complexes still representing, for these methods, a severe computational challenge.

For the description of the excited states and the optical spectra of transition metal tetrapyrrole complexes, the recently implemented TDDFT methods, which are first principle methods for the calculation of excitation energies and many related response properties

within a density functional context, have proven [36–43] to be an excellent alternative to conventional highly correlated ab initio methods. TDDFT methods do not demand a computational sense, compared with highly correlated ab initio methods, still they provide results which are usually competitive in accuracy with these approaches, as in the case of FBP, [36,38] Mgp, [37,42] and MgPz. [40]. A DFT related scheme, viz. DFT in conjunction with multireference configuration interaction (DFT/MRCI) has been successfully applied to the calculation of electronic absorption spectra of porphyrins, hydroporphyrins, porphyrazines and metalloporphyrins (MgP, ZnP) [44].

In this review, we will show that a full understanding of the electronic spectra of porphyrin and porphyrazine complexes, can be obtained combining the high accuracy of the TDDFT treatment of the excitation energies with a detailed analysis of the ground state electronic structure of these systems based on the Kohn–Sham (KS) molecular orbital (MO) model of DFT. Such important features as the relative intensities of the Q and B band systems, the nature of the higher energy additional bands, as well as the effect of the presence of metal 3d states, can all be rationalised.

The KS MO are physically meaningful (see Refs. [45,46] and references therein). This is related to the fact that the effective local potential of the KS model has as leading terms—apart from the nuclear potential and Coulomb potential of the total electronic density—the potentials due to both the Fermi (exchange) hole and the Coulomb hole [46–48]. The latter builds in effects of electronic correlation and in fact gives the KS MOs an advantage over Hartree–Fock orbitals in cases of strong near-degeneracy correlation. Virtual KS orbitals, being solutions in exactly the same potential as the occupied orbitals, have the advantage that they lack the artificial upshift and diffuse character of Hartree–Fock orbitals. The virtual-occupied KS orbital energy differences $\Delta\varepsilon_{ia} = \varepsilon_a - \varepsilon_i$ are in the TDDFT approach the zeroth-order approximation to the excitation energies. All these properties make the KS orbital model very suitable for interpretation of the electronic structure and elucidation of the character of the excitations. The meaning of KS orbitals and their use for interpretation of chemical bonding is extensively discussed in Ref. [49]. The use of KS orbitals affords a direct connection with the many LCAO-MO treatments based on semi-empirical or Hartree–Fock orbitals, while having at the same time the benefit of the high accuracy of the TDDFT treatment of the excitation energies.

We will first, in Section 3, discuss the electronic structure of MgP, ZnP, NiP, MgPz, ZnPz, and NiPz systems, taken as representative of nontransition and transition metal porphyrin and porphyrazine complexes.

A fragment approach with the four pyrrole rings and the methine or aza bridges as building blocks will be proven to be an useful tool to highlight the origin of the π ring orbitals and to understand the electronic differences between porphyrin and porphyrazine π ring systems.

The analysis of the π ring orbitals will be used in Section 4 to explain the intensity distribution in the Q/B band system of porphyrins. It will be elucidated how the time-honoured explanation of the intensity distribution in the Q and B bands of porphyrins from a simple polyene model can be reconciled with the actual structure of the ring systems being much more complicated.

In Section 5, the ground state electronic structure analysis of porphyrin and porphyrazine complexes will be extensively used for the interpretation of our TDDFT/Statistical Averaging of different Orbital-dependent model Potentials (SAOP) (vide infra) calculations of their optical spectra. In this section, we will also review the CASPT2 interpretation of the optical spectrum of MgP [35] and the TDDFT/B3LYP interpretation of the optical spectra of ZnP and ZnPz [43].

2. Method and computational details

2.1. Ground state calculations

DFT calculations have been performed with the Amsterdam Density Functional (ADF) program system [50–52] characterised by the use of a density fitting procedure to obtain accurate Coulomb and exchange potentials in each SCF cycle, by accurate and efficient numerical integration of the effective one-electron Hamiltonian matrix elements and by the possibility to freeze core orbitals.

For the exchange-correlation potential that appears in the KS equation, we use the recent model KS exchange-correlation potential v_{xc}^{SAOP} which is constructed with a statistical averaging of orbital dependent model potentials SAOP [53,54] (Section 2.2). We have also performed calculations using the more popular generalised gradient approximated potentials (GGA) by Becke (for exchange) [55] and Perdew (for correlation) [56], v_{xc}^{BP}. The absolute values of the one-electron energies change, of course, compared with SAOP results, in particular an upshift of the metal based MOs is observed, but the overall picture of the electronic structure remains substantially the same.

2.2. Excited state calculations

The computational method we use is based on the time-dependent extension of density functional theory. After initial applications by several authors [57–60], TDDFT has been given a firm basis by the Runge–Gross theorem [61]. TDDFT is thoroughly reviewed in

Refs. [62–65] and has been implemented in the mid-90s [66–71]. The excited state calculations have been performed with the ADF-RESPONSE module [72], which is an extension of ADF program system [50–52]. It has many features in common with the underlying ADF code and has similar scaling and parallelisation characteristics.

In the ADF-RESPONSE module implementation [68,72] the solution of the TDDFT response equations proceeds in an iterative fashion starting from the usual ground-state or zeroth-order KS equations. For these, one needs an approximation to the usual static xc potential $v_{xc}(r)$. After the ordinary KS equations have been solved, the first order density change is calculated from an iterative solution to the first order KS equations [68], where one needs an approximation to the so-called exchange–correlation kernel, the first functional derivative of the time-dependent xc potential $v_{xc}(\mathbf{r}, t)$ with respect to the time-dependent density $\rho(\mathbf{r}', t')$ [64,73,74].

$$f_{xc}(\mathbf{r}, \mathbf{r}', t, t') = \frac{\delta v_{xc}(\mathbf{r}, t)}{\delta \rho(\mathbf{r}', t')} \quad (1)$$

The quality of the excitation energy calculations has been shown to be primarily dependent on the quality of the KS potential, which should yield accurate orbital energies and in particular occupied-virtual energy differences, and of course the correct composition and asymptotic behaviour of the MOs. The SAOP potential has been designed to provide a correct $-1/r$, Coulombic asymptotic behaviour by using the LB94 potential with that behaviour in the outer region of the molecule [75]. In the inner atomic region, the required step like behaviour when going to inner shells and the intershell peaks are built in [47,76]. This special behaviour of the potential is achieved by making the local value of the potential explicitly dependent on the values of the (occupied) orbitals. It has been shown to provide a substantial improvement upon the local density approximation (LDA) and the standard generalised GGA in response calculations [54].

For the xc kernel, we use the Adiabatic Local Density Approximation (ALDA). In this approximation (used almost without exception in the applications of TDDFT), the time dependence (or frequency dependence, if one talks about the Fourier-transformed kernel) is neglected, and one simply uses the differentiated static LDA expression. In our case, we use the Vosko–Wilk–Nusair parameterisation [77]. This approximation is computationally efficient and it has been demonstrated [78] that the quality of the results depends strongly on the KS potential, the simple ALDA approximation proving to be quite adequate.

Excited state calculations have also been performed using the more popular GGA potential v_{xc}^{BP} employing Becke's gradient approximation for exchange [55] and Perdew's for correlation [56]. BP results, not reported here, are generally very similar to SAOP results, except for MLCT and LMCT excited states, which are computed at BP level at lower energy than at SAOP level as a consequence of the above mentioned upshift of the metal based MO on going from SAOP to BP potential. This leads in some cases to a different description of the excited states, the SAOP results appearing to be more in line with experiment than BP results.

The calculations have been performed for the spin allowed singlet A_{2u} and E_u excited states in the energy range covered by the experimental spectra, but only the E_u states will be reported and discussed in this paper. The A_{2u} excitations up to 5.0 eV have oscillator strengths smaller than 1.0×10^{-3} and are therefore, not relevant for the interpretation of the main spectral features of the investigated complexes.

2.3. Basis set and geometries

For the calculations, we made use of the standard ADF IV basis set [79] which is an uncontracted triple-ζ STO basis set, with one 3d polarisation function for C and N atoms, one 3p and one 3d for Mg atom, one 2p for H atoms, and a triple-ζ nd, $(n+1)$s basis with one $(n+1)$p function for Zn and Ni. The cores (C, O: 1s; Mg, Zn, Ni: 1s-2p) were kept frozen.

In the calculations, we have used the ground state optimised structures, obtained with Becke–Perdew xc functional, imposing D_{4h} symmetry. The molecules lie in the xy plane, with the x- and y-axes passing through pyrrolic nitrogens (cf. Fig. 1). Selected optimised structural data of the investigated MP and MPz series obtained at BP level is reported in Table 1. They show good agreement with other recent DFT calculations on MgP [80–83], ZnP [43,80] and ZnPz [43], which are also of D_{4h} symmetry. As for NiP, DFT/B3LYP calculations by Kozlowski et al. [84] show that the planar structure is unstable with respect to ruffling although the potential is soft and easily overcome by intermolecular forces. The lowest energy structure of NiP is found by these authors

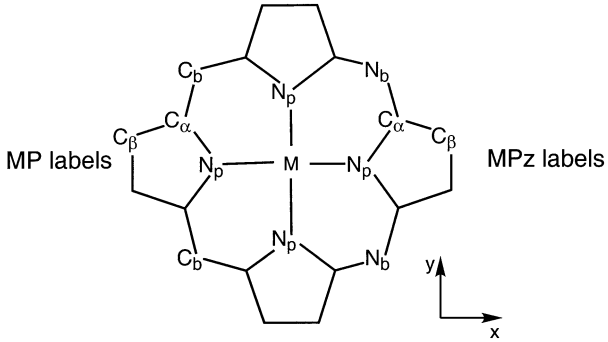

Fig. 1. Atom labelling scheme for MP (left side) and MPz (right side).

Table 1
Optimised bond distances (Å) and angles (°) for MPs and MPzs (M = Mg, Zn, Ni)

	MgP [a]	ZnP [b]	NiP [c]	NiP [d]	MgPz [c]	ZnPz [b]	NiPz [c]
Bond distances							
M–Np	2.064	2.056	1.972	1.951(2)	1.998	1.981	1.894
N_p–C_α	1.376	1.376	1.383	1.379(2)	1.371	1.373	1.382
C_α–C_β	1.448	1.447	1.440	1.435(4)	1.463	1.461	1.451
C_β–C_β	1.369	1.367	1.362	1.347(3)	1.366	1.364	1.358
C_α–C_b (N_b)	1.402	1.399	1.381	1.371(3)	1.345	1.340	1.325
Bond angles							
C_α–C_b(N_b)–C_α	127.3	126.9	123.7	123.5(2)	124.1	123.5	120.3
C_α–N_p–C_α	107.0	107.0	104.7	104.3(2)	108.9	108.4	105.8
C_β–C_α–N_p	109.6	109.6	111.0	111.0(3)	108.3	108.6	110.1
C_β–C_β–C_α	106.9	107.0	106.7	106.8(2)	107.2	107.2	106.9

The geometrical parameters calculated for NiP are compared with the experimental ones.
[a] Ref. [42].
[b] Ref. [100].
[c] Ref. [40].
[d] Experimental data from Ref. [86] (the numbers in parentheses are the estimated standard deviations).

to be a true minimum with D_{2d} symmetry. The extent of the distortion is small as is the energy gain (−0.1 kCal mol^{-1}) and most importantly depends on the level of theory (quality of the basis set). At BP level we find that the extent of the distortion in the D_{2d} structure is negligible, as is the energy gain (−0.03 kCal mol^{-1}) [85]. The dihedral angle between the C_α–N bonds on adjacent pyrrole rings, which is a sensible measure of the ruffling is only 2.3° [85], much less than the −20° calculated by Kozlowski et al. [84] at the B3LYP level of theory, but very close to the experimental value of −2° determined by Jentzen et al. [86]. Actually, these authors, based on similarities of the resonance Raman spectra of NiP in the single crystal and in solution, suggest that NiP exists only in the planar conformation. As inferred from the data of Table 1 our D_{4h} structure is in good agreement with the averaged planar D_{4h} structure reported by Jentzen et al.

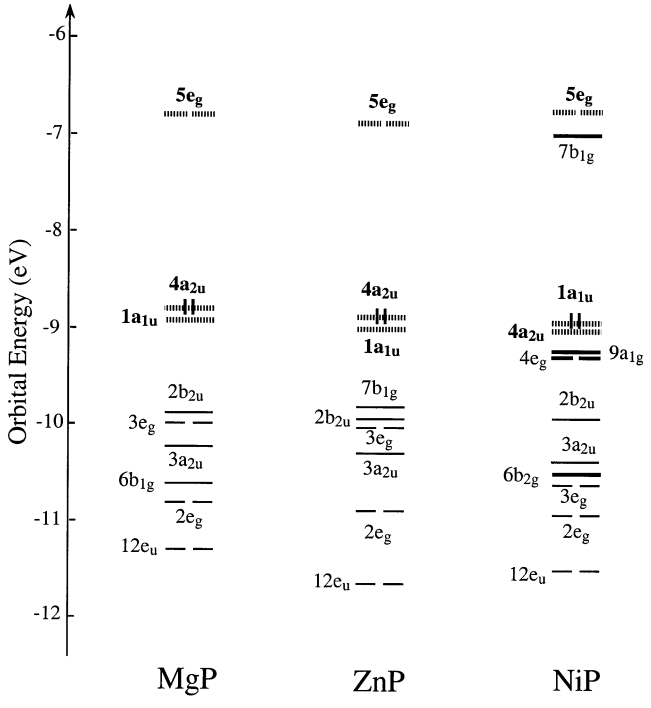

Fig. 2. Energy level scheme for MgP, ZnP, and NiP. Double occupancy is indicated for the HOMO only. All lower-lying levels are also doubly occupied. The metal 3d orbitals are indicated with heavy lines, and the four Gouterman orbitals are indicated with hatched lines.

3. Ground state electronic structure analysis

3.1. The π system of porphin and porphyrazine

The highest occupied and the lowest unoccupied ground state one-electron levels of MPs and MPzs (M = Mg, Zn, Ni) are shown in Figs. 2 and 3, respectively. For ease of comparison, we adopt for all systems the same numbers for the e_g and a_{2u} levels in the various compounds that are similar. Specifically, the occupied $3e_g$ and the unoccupied $5e_g$ levels are in all systems the same type of π ring orbitals, to be explained below. There is a $4e_g$ orbital (of $3d_\pi$ type) in between the $3e_g$ and $5e_g$ levels in the Ni systems, but not in the Mg and Zn systems. In ZnP and ZnPz there is a lower lying $3d_\pi$ orbital, but it is ignored for the numbering of the $3e_g$ and $5e_g$. In the same way, in the numbering of the a_{2u} levels the occupied $3p_z$ in Zn and Ni, of a_{2u} symmetry, is counted, resulting in the number $3a_{2u}$ for the lowest a_{2u} orbital in Figs. 2 and 3. In the Mg system the corresponding a_{2u} level is also given the number 3 even though there is no lower lying $3p_z$.

Most of the features of the orbital level spectrum and the underlying electronic structure of the π ring systems

can be understood from a fragment approach where we take as building blocks the four pyrrolic rings and the methine or aza bridges.

The pyrrolic rings are basically cyclopentadiene (Cp) rings perturbed by the N substitution in the five-ring. Referring to the C_{5v} nomenclature appropriate for the Cp ring, we note that the pyrrolic π electron system is characterised by a lowest A_1 combination, with, however, relatively large weight on the more electronegative N atom (see Fig. 4), followed by the E_1 set of orbitals, which are no longer degenerate, the 'e_x' partner with amplitude on N (and on the C_β carbon atoms) being more stabilised (by 1.12 eV) than the 'e_y' partner with N in its nodal plane and high amplitude on the C_α atoms. The distinguishing feature of the 'e_x' and 'e_y' orbitals is the different amplitudes on the C_α atoms, to which the methine or aza bridges will attach. The nodal plane of the 'e_x' orbital passes practically through the C_α atoms, which therefore, have no amplitude, so we may expect little interaction with the methine or aza bridges. On the other hand, the 'e_y' orbitals with their large C_α amplitudes will strongly interact with the bridges. The E_2 orbitals finally are also split by the N perturbation, but less so (only 0.55 eV) than the E_1 set. The $e_{x^2-y^2}$ has relatively large amplitude on C_α, and may therefore, play a role in the interaction with the bridges.

When forming the $(Py)_4$ cage, without bridges present, the MOs of the Py rings form the symmetry combinations as indicated in Fig. 4. Evidently, the high C_α amplitudes lead to significantly more overlap and energy dispersion for the 'e_y' and '$e_{x^2-y^2}$' orbitals than for the other ones.

We next consider the interaction of the $(Py)_4$ orbitals with methine and aza bridges in Figs. 5 and 6, respectively. Note that we take as electron count for the $(Py)_4$ cage 22 electrons. The four times five π electrons for the neutral rings are supplemented with two electrons, which would make the $3e_g$ level in Fig. 4 fully occupied and give the $(Py)_4$ system a $2-$ charge, in accordance with the closed shell nature of the $(Py)_4$ system in the P^{2-} and Pz^{2-} rings (see below and see Fig. 5). In the metal salts the metal ion has accordingly charge $2+$. In FBP the two additional electrons are supplied by the two in-plane hydrogen atoms and are neutralised by the two proton charges.

A notable feature in the interaction diagram for $(Py)_4$ with $(CH)_4$ in Fig. 5 is that the 'e_x' orbitals, with their lack of amplitude on C_α, are very little affected by the bridges and carry over almost unperturbed to the porphin ring system. The mixing percentages with

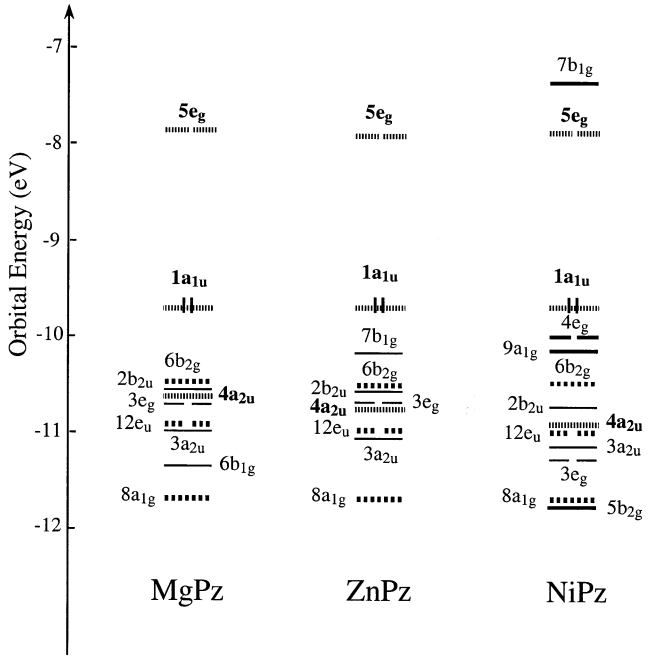

Fig. 3. Energy level scheme for MgPz, ZnPz, and NiPz. Double occupancy is indicated for the HOMO only. All lower-lying levels are also doubly occupied. The metal 3d orbitals are indicated with heavy lines, the four Gouterman orbitals are indicated with hatched lines, and the N_b lone pair orbitals of a_{1g}, b_{2g} and e_u symmetry are indicated with dashed lines.

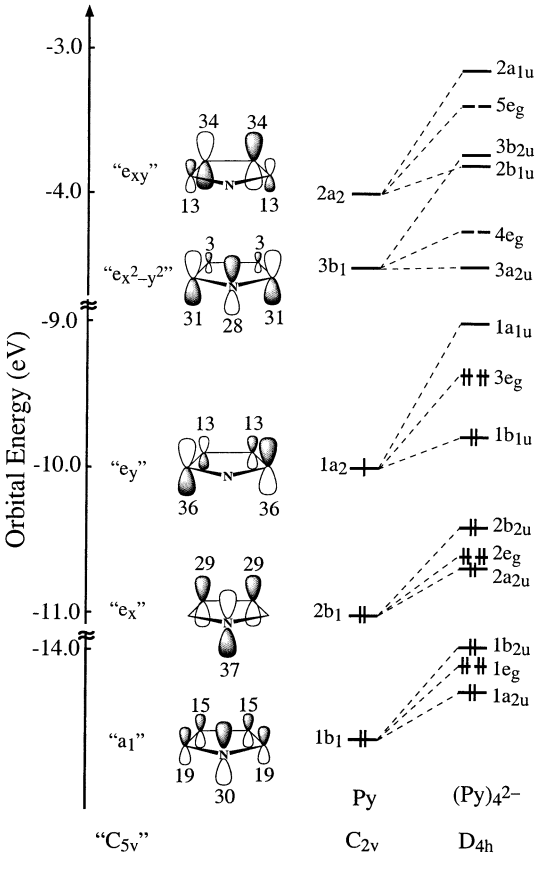

Fig. 4. Orbitals and orbital energies of the pyrrolic ring system. The contributions of the individual C and N p_π atomic orbitals to the MOs, in percentages based on Mulliken gross orbital populations per MO, are indicated in the Figure. The orbital levels in the $(Py)_4$ cage are also given. These have been calculated for the neutral $(Py)_4$ system, but the orbital occupations are indicated for the closed shell $(Py)_4^{2-}$ system.

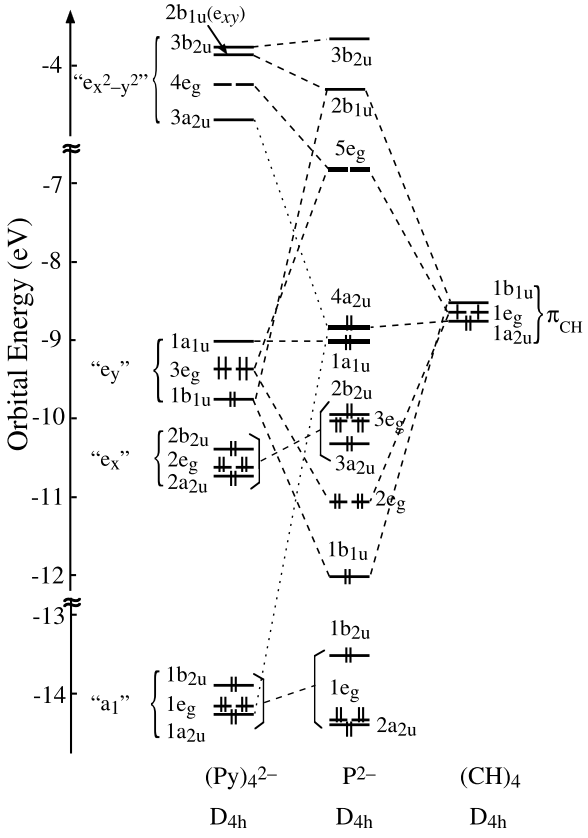

Fig. 5. Orbital interaction diagram for interaction between the $(Py)_4^{2-}$ cage and the four CH methine bridges. Gouterman's four orbitals ($1a_{1u}$, $4a_{2u}$, $5e_{g,xz}$, $5e_{g,yz}$) are indicated with hatched lines. The orbital numbering of the P ring system has been adapted to the situation in metal salts (see Fig. 2).

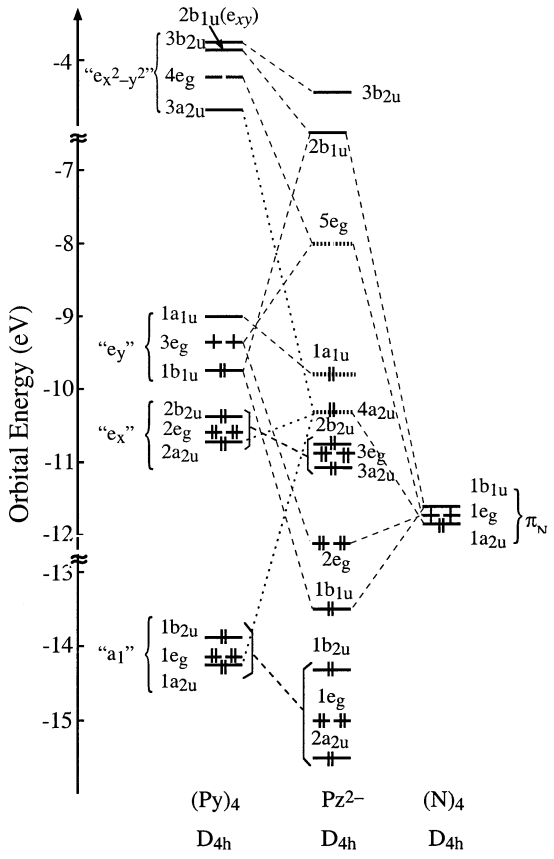

Fig. 6. Orbital interaction diagram for interaction between the $(Py)_4$ cage and the four N bridging atoms. Gouterman's four orbitals ($1a_{1u}$, $4a_{2u}$, $5e_{g,xz}$, $5e_{g,yz}$) are indicated with hatched lines. The orbital numbering of the Pz ring system has been adapted to the situation in metal salts (see Fig. 3).

$(CH)_4$ orbitals are quite low, being 3 and 2% for the $1e_g$-$(CH)_4$ and $1a_{2u}$-$(CH)_4$ into the $3e_g$-P and $3a_{2u}$-P, respectively, ($2b_{2u}$-P is 100% $2b_{2u}$-$(Py)_4$).

The $2b_{2u}$, $3e_g$, $3a_{2u}$ set of 'e_x' orbitals can be clearly recognised in the levels of the metal salts in Figs. 2 and 3. We have for ease of comparison adopted the same orbital numbers in Figs. 5 and 6 as in the complexes in Figs. 2 and 3, so the numbers of the a_{2u} orbitals of P and Pz have been raised by 1 and the first virtual e_g orbital has been numbered $5e_g$.

Comparing the porphyrin complex levels in Fig. 2 with the P levels in Fig. 5 we note that the 'e_x' set of orbitals remains almost unaltered in MgP and ZnP, and is only partially disturbed by the presence of the transition metal ion in NiP where the $3e_g$ is pushed down, to below the $3a_{2u}$, by the Ni $3d_\pi$ which enters the orbital energy diagram as $4e_g$, above the 'e_x' set. The metal orbital $3d_{xy}(6b_{2g})$ is inserted in the 'e_x' set. The plot of the $3a_{2u}$ orbital of NiP in Fig. 7 nicely demonstrates its 'e_x' origin, with large amplitude at the pyrrolic nitrogens and (with opposite sign) at the C_β atoms.

Contrary to the 'e_x' orbitals, the 'e_y' orbitals exhibit strong interaction with the CH bridges. The $(Py)_4$ $3e_g$–e_y and $1b_{1u}$–e_y orbitals show interaction with orbitals of matching symmetry in the set of $(CH)_4$ π-orbitals, resulting in large gaps between the bonding and antibonding combinations. The antibonding ones, $5e_g$ and $2b_{1u}$, actually rise so high as to come close to the '$e_{x^2-y^2}$' and 'e_{xy}' type of orbitals and are stabilised by admixture

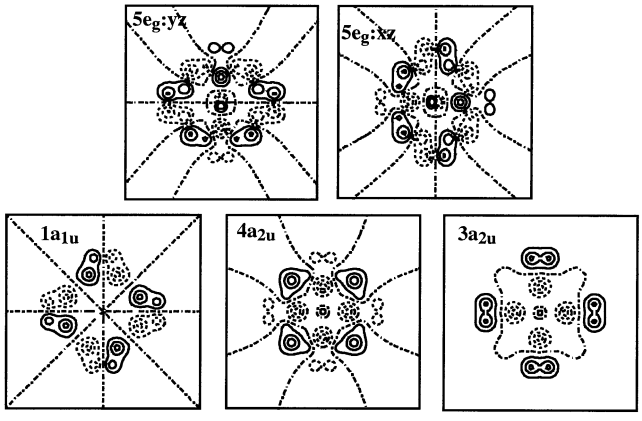

Fig. 7. Contour plots of the $1a_{1u}$, $3a_{2u}$, $4a_{2u}$, $5e_{g,xz}$, $5e_{g,yz}$ orbitals of NiP, The plane of drawing is 0.3 Bohr above the molecular plane. Contour values are 0.0, ±0.05, ±0.1, ±0.2, ±0.5(e bohr^3)$^{1/2}$.

of these. The $5e_g$ LUMO is of course important for the low-lying excitation energies. Interestingly, the two highest occupied orbitals are also derived from the 'e_y' and π_{CH}-orbitals, but from the two orbitals, $1a_{1u}$ on $(Py)_4$ and $1a_{2u}$ on $(CH)_4$, that find no partner on the other system. These therefore, end up in P as 'nonbonding' orbitals at almost unchanged energies. The $1a_{1u}$ has nodal planes through the CH bridges and is virtually a 100% $(Py)_4$-e_y orbital. Its 'e_y' origin and lack of amplitude at the bridges are evident from the orbital plot of the $1a_{1u}$ of NiP in Fig. 7. The $4a_{2u}$ is an in-phase combination of the π-orbitals on the C atoms of the CH bridges (the A_{2u} irrep is only antisymmetric with respect to the plane of the molecule). It does in fact have significant admixture of the $3a_{2u}$ and $1a_{2u}$ $(Py)_4$ orbitals (23 and 14%, respectively), which both have amplitude at C_α. The lack of C_α character prevents the $(Py)_4e_x$–$2a_{2u}$ to get involved. It is easily deduced from the phases with which the $3a_{2u}$-$(Py)_4$ and $1a_{2u}$-$(Py)_4$ will mix with the $1a_{2u}$-$(CH)_4$, that the amplitudes on the pyrrolic N_p will reinforce each other, the amplitudes at C_α, however, interfering destructively. The plot of the $4a_{2u}$ of NiP in Fig. 7 indeed exhibits in addition to the strong amplitude at the CH bridges of this originally $-(CH)_4$ orbital, considerable amplitude with reversed sign at the N_p.

The plots of Fig. 7 further demonstrate that the $5e_g$ orbitals consist of antibonding combinations of the $(Py)_4$'e_y'–$3e_g$ (37%) with the $(CH)_4$ $1e_g$ (29%), stabilised by the $(Py)_4$ '$e_{x^2-y^2}$'–$4e_g$ (27%). The 'e_y'–$3e_g$ and '$e_{x^2-y^2}$'–$4e_g$ are localised on different sets of Py rings, for instance $e_{g,xz}$ combinations are formed with 'e_y' orbitals on Py rings at the y axis, and with '$e_{x^2-y^2}$' orbitals on the Py rings at the x-axis. Admixture of '$e_{x^2-y^2}$'–$4e_g$ thus brings in amplitude on the N_p and C_α atoms of the two other Py rings than where 'e_y'–$3e_g$ was located (cf. Fig. 7).

The remaining levels in Fig. 2 ($12e_u$, $6b_{1g}$ etc.) are not of π type but have in-plane character and will be discussed in the next subsection.

Fig. 6 displays the orbital interaction diagram for $(Py)_4$ interaction with $(N)_4$. The interaction pattern is very similar to the one for interaction with $(CH)_4$, in particular again the 'e_x' set of $(Py)_4$ orbitals has little interaction with the bridging N atoms, and the 'e_y' set strongly interacts, resulting in a large gap between the bonding $1b_{1u}$ and $2e_g$ orbitals and the antibonding partners $5e_g$ and $2b_{1u}$. The latter are stabilised by admixture of the '$e_{x^2-y^2}$'–$4e_g$ and 'e_{xy}'–$2b_{1u}$.

An important difference between the aza and methine bridges is the higher electronegativity of the former, resulting in an energetically lower lying set of $(N)_4$ p_π orbitals. As a consequence the final charge distribution on $(N)_4$ will be more negative, and on $(Py)_4$ more positive. This is visible in the shift in the energies of $(Py)_4$ orbitals that do not interact strongly, such as the low-lying 'a_1' set and the 'e_x' set: they all shift downwards due to the resulting positive charge on $(Py)_4$. This also holds for the 'e_y'–$1a_{1u}$ which is in the Pz ring system a pure $(Py)_4$ orbital, as it is in the P ring system. We note that the N_b-based $4a_{2u}$ is no longer degenerate with the $1a_{1u}$, it is even more stabilised. This is due to the much lower energy of the N_b based p_π orbitals than the CH p_π orbitals. The negative charging of the N_b atoms actually causes the $4a_{2u}$ to shift up considerably with respect to the initial atomic $(N)_4$ levels, but this upward shift combined with the downward shift of the $1a_{1u}$ is still not sufficient to bring $4a_{2u}$ close to $1a_{1u}$, there is still a considerable gap. Incidentally, the $4a_{2u}$ is not purely located at the bridging atoms, it has 47% $(N)_4$-$1a_{2u}$ character, and 16, 22 and 15% admixtures of 1, 2 and $3a_{2u}$ orbitals of $(Py)_4$. This orbital is actually, apart from its lower energy, rather similar to the $4a_{2u}$ of P, with large amplitude at the bridges but also significant amplitude at the N_p atoms (see Fig. 7).

When comparing the Pz level scheme of Fig. 6 to the level scheme of porphyrazine complexes in Fig. 3 we note that the gap between the $1a_{1u}$ and $4a_{2u}$ orbitals is even considerably enhanced in the metal salts where the $4a_{2u}$ orbital shifts below the $2b_{2u}$, although it is still above $3a_{2u}$, so it becomes embedded in the 'e_x' set of orbitals. In the metal salts, specially in NiPz, the $4a_{2u}$ is indeed stabilised by interaction with the metal p_z–a_{2u} orbital ($3p_z$ for Mg, $4p_z$ for Zn and Ni). In NiPz the $3e_g$ orbitals belonging to this set are stabilised strongly by the metal $3d_\pi$–$4e_g$ so that they end up below $3a_{2u}$.

3.2. The N_p and N_b lone pairs

In addition to the π levels discussed above, there are the in-plane levels derived from the N_p and—in the porphyrazines—the N_b lone pairs. The N_p lone pairs yield combinations of A_{1g}, B_{1g} and E_u symmetry. In the level scheme of Fig. 2 the $12e_u$ (all MP systems) can be recognised, as well as the $6b_{1g}$ (MgP) and $7b_{1g}$ (ZnP). In NiP the N_p-derived b_{1g} orbital is so strongly stabilised by σ interaction with the Ni $3d_{x^2-y^2}$ orbital (the strongly destabilised $7b_{1g}$) that it is not visible in the diagram. The totally symmetric a_{1g} combination of N_p lone pairs is also at too low energy to enter the diagram. In the MPz systems (Fig. 3) the N_b lone pair orbitals, which have A_{1g}, B_{1g} and E_u symmetry, are at higher energy than the N_p lone pairs, the latter undergoing the general downshift of pyrrolic levels due to the positive charge. The N_b lone pair orbitals are the $6b_{2g}$, $12e_u$ and $8a_{1g}$: they are distinguished in Fig. 3 by hatched lines. We note that the N_p lone pairs do no longer enter the diagram except for the $6b_{1g}$ (MgPz) and $7b_{1g}$ (ZnPz), since the other ones are too much downshifted by the interaction with the higher lying N_b lone pair orbitals of the same symmetry (the $12e_u$ and the $8a_{1g}$).

3.3. The metal 3d levels

An important feature in the NiP and NiPz MO levels of Figs. 2 and 3 is the presence of the metal 3d orbitals, which are denoted by heavy lines. The Zn-3d shell remains indeed almost unperturbed in the low energy region of the orbital spectrum, the only 3d orbital which interacts to some extent with the macrocycles being, as mentioned the $3d_{x^2-y^2}$. In the virtual spectrum of the Ni systems there is the $d_{x^2-y^2}$, $7b_{1g}$, which is pushed up by antibonding with the pyrrolic N_p lone pairs of B_{1g} symmetry. The highest occupied 3d levels are the d_{z^2}, $9a_{1g}$, and the $d_{xz,yz}$, $4e_g$. These $3d_\pi$ are strongly mixed with the lower lying N_p based π-orbitals of the macrocycle, the 'e_x'–$3e_g$. The strength of the σ interaction between the tetrapyrrole N_p lone pairs and the Ni $d_{x^2-y^2}$, as well as of the out-of-plane interaction between the tetrapyrrole N_p p_z and the Ni-d_π provide two examples of sensitivity to the macrocycle framework which are worth noting. Both these interactions, but specially the former, are stronger, the smaller the coordinating cavity of the macrocycle is. As a matter of fact in NiPz, where the hole size is smaller than in NiP (the M–N_p distance is 1.894 Å in NiPz, 1.972 Å in NiP), the σ antibonding $7b_{1g}$ orbital is more strongly destabilised and lies above the $5e_g$, and the splitting of the metal-macrocycle π bonding/antibonding pair ($3e_g$/$4e_g$) is slightly larger than in the porphyrin analog.

As for the remaining occupied 3d orbital, the in-plane d_{xy} is an almost purely 3d orbital in NiP where the $6b_{2g}$ has a 93% d_{xy} character. In NiPz the $3d_{xy}$, $5b_{2g}$, is at considerably lower energy, being pushed down by the NiPz-$6b_{2g}$ which is a predominantly N_b lone pair orbital but also contains some N_p in plane p_π character which makes it suitable for in plane π-interaction with the metal $3d_{xy}$.

An extensive discussion of all the metal-macrocycle orbital interactions in porphyrin, porphyrazine and related tetrapyrrole complexes has been given in Refs. [87,88].

4. Intensity distribution in the Q/B band system of porphyrins

4.1. Fragment analysis and transition dipole moments

The highest occupied orbitals $1a_{1u}$ and $4a_{2u}$, and the lowest unoccupied orbitals $5e_{g,xz}$ and $5e_{g,yz}$ are the four orbitals whose significance for the UV–vis absorption spectrum have been stressed by Gouterman [15]. The high absorption intensities (at low excitation energy) of these transitions as well as the much lower intensities for other transitions such as those involving orbitals derived from other Py orbitals like the 'e_x' set, can be rationalised as follows. The Q and B bands consist of transitions involving orbitals that all derive from the same orbitals at the $(Py)_4$ side (the 'e_y' set) and the $(CH)_4$ side (the π_{CH}-orbitals). The transition energies are low since we are dealing with excitations out of nonbonding (nonstabilised) orbitals to antibonding ones. The intensities are high due to large transition dipole matrix elements. This is typical for transitions between orbitals derived from the same MOs on the fragments (pyrrole say) and when there is considerable spacing between the fragments. This means that when a transition dipole matrix element is nonzero by symmetry, it will usually be large since the intra-unit (on one Py fragment, or on one CH fragment) contributions will be large. We may take as an example the y-components of the E_u excited states, ignoring spin for the moment (i.e. assuming the electrons to be singlet coupled). Both the $1a_{1u} \rightarrow 5e_g$ and the $4a_{2u} \rightarrow 5e_g$ excitations lead to E_u states, the E_u–y components being $le_{u,y} = 1a_{1u}5e_{g,xz}$ and $2e_{u,y} = 4a_{2u}5e_{g,yz}$. The dipole matrix element $\langle 1a_{1u} \mid y \mid 5e_{g,xz} \rangle$ is large because the $1a_{1u}$ consists of 'e_y' orbitals on $(Py)_4$ while $5e_{g,xz}$ also has, apart from the antibonding π_{CH} contribution, 'e_y' character, namely on the Py groups at the positive and negative y-axes (see Fig. 7). The on-site overlaps (on these Py fragments) are large (in fact maximally large since the same 'e_y' orbitals occur in $1a_{1u}$ and $5e_{g,xz}$). The multiplication with y takes care that the signs are such that constructive interference occurs. Moreover it effectively introduces a multiplying factor of order of magnitude of 7 a.u. (roughly the distance of the origin to a pyrrolic centroid) in the overlap integrals. The other dipole matrix element, $\langle 4a_{2u} \mid y \mid 5e_{g,yz} \rangle$, is large because both $4a_{2u}$ and $5e_{g,yz}$ have as important constituents the same set of orbitals, i.e. the π_{CH}. We may expect the dipole matrix element to be somewhat less than for $\langle 1a_{1u} \mid y \mid 5e_{g,xz} \rangle$ since the $4a_{2u}$ has less π_{CH} content (59%) than $1a_{1u}$ has 'e_y' content (98%), and $5e_{g,yz}$ has less π_{CH} content (29%) than $5e_{g,xz}$ has 'e_y' content (37%). The situation is actually more favourable for $(4a_{2u} \mid y \mid 5e_{g,yz})$ than this comparison suggests, since the N_p p_z character that both the $4a_{2u}$ (due to the $(Py)_4$-$3a_{2u}$ and $(Py)_4$-$1a_{2u}$ admixtures, see above) and the $5e_{g,yz}$ (due to $(Py)_4$-$4e_{g,yz}$ admixture) acquire, are helpful for building a large dipole matrix element, as may be easily deduced from the phases as depicted in Fig. 7. We find numerically in NiP the large value of ca. 3.25 a.u. for $\langle 1a_{1u} \mid y \mid 5e_{g,xz} \rangle$ and the $\langle 4a_{2u} \mid y \mid 5e_{g,yz} \rangle$ matrix element is, with ca. 2.92 a.u. actually not much smaller. In free-base porphin the analogous values are 3.30 and 2.72 a.u., respectively.

For excitations out of the 'e_x'-derived set of orbitals, $2b_{2u}$, $3e_g$ and $3a_{2u}$, to $5e_g$ orbitals, the dipole matrix elements will not benefit from the factors that lead to high intensity of the Gouterman transitions. The 'e_x' orbitals have zero on-site overlap with the 'e_y' orbitals that constitute the $5e_g$ orbitals. The dipole operator will

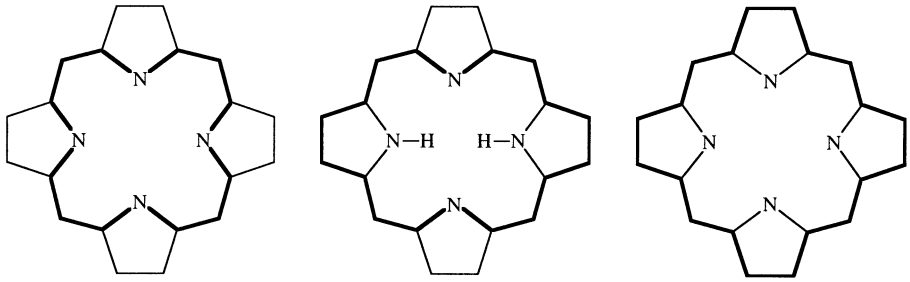

Fig. 8. Conjugation pathway in the basic porphyrin ring, (a) 16-membered ring system; (b) 18-membered ring system; (c) 20-membered ring system.

therefore, not work as an enhancement factor roughly proportional to the dimension of the ring system, but intensity has to derive from the dipole operator acting within a pyrrole fragment to produce a finite transition dipole matrix element in the same way as it would in an isolated pyrrole ring. For example, let us consider the transition $3a_{2u} \rightarrow 5e_{g,yz}$. The transition dipole matrix element $\langle 3a_{2u} \mid y \mid 5e_{g,yz} \rangle$ will for the Py rings at the plus and minus x axes (the horizontal axis in Fig. 7) be the $\langle e_x \mid y \mid e_y \rangle$ matrix element of pyrrole, which will be quite small. The dipole matrix elements will also benefit from the fact that the 'e_x' orbitals have large N_p amplitude while we have seen that also $5e_g$ acquires some N_p character. This will lead to contributions to $\langle 3a_{2u} \mid y \mid 5e_{g,yz} \rangle$ coming from the large N_p amplitudes at the plus and minus y axes of $3a_{2u}$ and $5e_{g,yz}$, see Fig. 7. So the dipole matrix elements for excitations from 'e_x' orbitals to $5e_g$ will not be zero (except for $3e_g \rightarrow 5e_g$, where they are zero by symmetry). Nevertheless, we find dipole matrix elements that are smaller by factors between 3 and 20 compared with the large dipole matrix elements for the Gouterman transitions.

We note that these intensity considerations are not particular to the porphyrins but will hold very generally for composite systems. In particular it transpires that high intensity in a composite system may occur, as it does here for the Gouterman transitions, irrespective of the constituting fragments themselves being strong chromophores or not, since the mechanism for intensity does not rely on large dipole matrix elements for the isolated fragments.

The proximity of the $1a_{1u}$ and $4a_{2u}$ levels suggests near-degeneracy of the two primary E_u excited states derived from the $(1a_{1u}5e_g)$ and $(4a_{2u}5e_g)$ configurations. In case of accidental degeneracy or near-degeneracy already a small coupling matrix element will induce strong mixing, close to 50–50. There is a vast literature on the importance of this configuration interaction between the $(1a_{1u}5e_g)$ and $(4a_{2u}5e_g)$ configurations. The phases of the mixing coefficient and the transition dipoles are such that the low-energy stabilised linear combinations, accounting for the Q bands in the visible spectrum, have low intensity due to opposite directions of the two large transition dipoles, while the high-energy out-of-phase linear combination, accounting for the B or Soret band in the UV, has parallel transition dipoles and therefore a large overall transition dipole, i.e. high intensity. A qualitative understanding of the main spectral features of the porphin spectra is thus obtained straightforwardly. We should of course be aware of the possibility of further configuration interaction, which will in practice bring contributions from 'e_x' to $5e_g$ transitions (the $2b_{2u} \rightarrow 5e_g$ and $3a_{2u} \rightarrow 5e_g$ being the only allowed ones), but also from for instance $3e_g \rightarrow 2b_{1u}$ and other transitions. We will consider in Section 5 the detailed results of the calculations.

4.2. The cyclic polyene model revisited

It may be worthwhile to briefly consider the connection of our presentation in terms of pyrrolic fragments and CH bridges with the interpretation of the porphin spectra starting from a cyclic polyene model system, which has historically played a large role [16,18,19] and is still often cited as providing a qualitative basis for our understanding of the weak Q and strong B band system of porphyrins. The cyclic polyene model has its roots in the work of Simpson [18] who pointed out that it affords a natural explanation for the intensities of the Q/B band system. Taking a regular 16-membered aromatic ring system (modelling for instance the 16 atoms of the inner ring system of porphin, including the pyrrolic N_p and C_α atoms and the bridges (see Fig. 8a) and 18 π electrons, the D_{16h} symmetry of the system leads to a configuration $(a_{2u})^2(e_{1g})^4(e_{2u})^4(e_{3g})^4(e_{4u})^4(e_{5g})^0$. The highest occupied level is degenerate, the two orbitals being characterised by four vertical nodal planes. The LUMOs are characterised by five nodal planes. The excited configuration $(e_{4u})^3(e_{5g})^1$ gives rise to an E_{1u} and an E_{9u} excited state. The dipole operator having E_{1u} symmetry, excitation from the A_{1g} ground state is allowed to E_{1u} (to be associated with the B band) and forbidden to E_{9u} (Q band). The argument remains unaltered if the cyclic polyene model would contain, as

has also been argued (see below), 18 or 20 CH groups and accordingly D_{18h} or D_{20h} symmetry. It was actually realised [18] that even the simple free-electron model of particles on a ring, with doubly degenerate states of angular momentum λ, $\Phi_{\lambda,m} = 1/\sqrt{2\pi}e^{im\varphi}$, $m = \pm\lambda$, would lead to a similar result. The ground state configuration $(\lambda = 4)^4(\lambda = 5)^0$ would lead, by simple angular momentum coupling (Platt's [19] 'vector model'), to excited states with $\Lambda = 1$ and 9, transitions to the former being allowed and to the latter being forbidden.

The cyclic polyene model had some difficulties. Early MO calculations of Hückel type did not agree with it, in that the two highest occupied orbitals of the porphin ring system, a_{1u} and a_{2u} in D_{4h} symmetry, proved not be degenerate. It was also not clear why the conjugated system of the porphin ring would not include the full number of 24 atoms. Considerable attention has been devoted to these questions, for instance, to arguments why some of the outer (C_β) carbon atoms would not be conjugated, and neither some of the pyrrolic N_p atoms. For instance, FBP has been depicted as having an 18-membered conjugated system [18], (see Fig. 8b). Alternatively, attempts have been made to remove the pyrrolic N_p atoms from the conjugated system, for instance, by changing its Hückel parameters significantly, so that a 20-membered ring would remain [17] (see Fig. 8c). It has also been argued that the inner 16-membered ring (see Fig. 8a) is the main path of conjugation [14,89,90]. The specific simplifications that have been introduced, such as the neglect of the outer two of the five atoms of the pyrrolic five-ring in the conjugated system, and either the neglect of the difference between a carbon atom and the N hetero-atom in the pyrrolic rings or the total removal of the N_p from the conjugation, seem hard to justify. Indeed, recent calculations [91,92] of nuclear magnetic shieldings, interpreted in terms of induced ring currents, have come to the conclusion that the outer C_2H_2 units of the Py rings are not exocyclic bridges but they participate in the aromatic pathway, which appears to include all 26 π electrons of the P^{2-} ring system.

It is nevertheless to be noted that the cyclic polyene model does have elements of truth. The highest occupied levels, $1a_{1u}$ and $4a_{2u}$, do have four nodal surfaces, as E_{4u} levels would (see Fig. 7). The $5e_g$ has five nodal surfaces. The $(1a_{1u}5e_g)$ and $(4a_{2u}5e_g)$ configurations do exhibit strong configuration mixing, which, being not symmetry dictated as in the cyclic polyene model, arises from a two-electron coupling matrix element between the nearly degenerate excitations. This configuration mixing explains the intensity distribution over the Q/B band systems (see above) in a manner that is analogous to the symmetry based argument of the cyclic polyene model. It is, therefore, understandable that it has been felt that

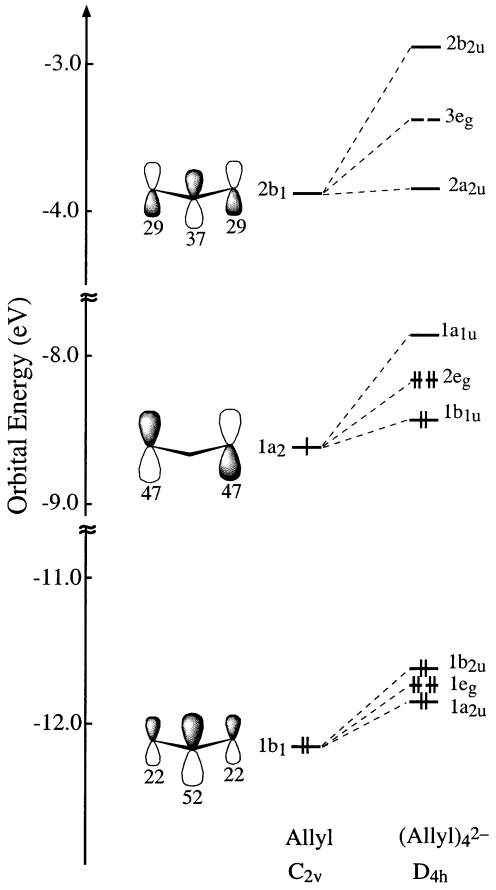

Fig. 9. π orbitals and orbital energies of the allyl. The contributions of the individual C p_z atomic orbitals to the MOs, in percentages based on Mulliken gross orbital populations per MO, are indicated in the Figure. The orbital levels in the $(Allyl)_4$ cage are also given (levels calculated for neutral $(Allyl)_4$ but orbital occupations indicated for closed shell $(Allyl)_4^{2-}$).

the cyclic polyene model (or even a free-electron ring model) must capture an essential electronic structure feature of the porphin ring system.

Can it really been maintained that the Q/B band system, and the small intensity of the Q band, are to be understood from an underlying D_{16h} (or higher D_{nh}) symmetry? We feel that the cyclic polyene model abstracts so far from reality that it at the same time offers a new problem, namely the question how we can understand why it works so well. This question can in fact be answered from the insights we have gained so far. Let us consider replacing the pyrrolic rings by allylic groups, to obtain a 16-membered cyclic polyene. Allyl also has C_{2v} symmetry and it has, as does the Py ring, a lowest occupied $1b_1$ orbital (see Fig. 9). There is no 'e_x' orbital, but there is the well known singly occupied allyl $1a_2$ orbital, with a nodal plane through the central C atom, which will act like the 'e_y' orbital of Py, having large amplitude on the peripheral C atoms that will connect to the CH bridges. Finally there is a b_1 virtual orbital, analogous to the '$e_{x^2-y^2}$' of Py. The $(allyl)_4$

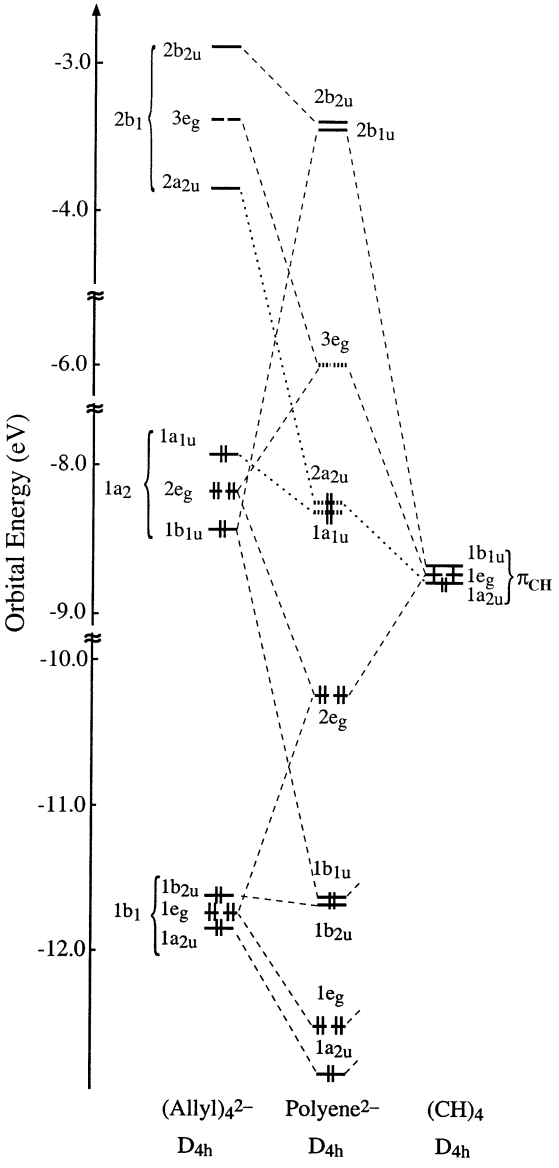

Fig. 10. Orbital interaction diagram for interaction between the $(Allyl)_4^{2-}$ cage and the four CH methine bridges. Gouterman's four orbitals ($1a_{1u}$, $2a_{2u}$, $3e_{g,xz}$, $3e_{g,yz}$) are indicated with hatched lines.

orbital scheme of Fig. 9 is perfectly analogous to the one of $(Py)_4$ in Fig. 4 without of course the set of 'e_x' derived orbitals. Switching on the interaction of the $(allyl)_4$ cage with $(CH)_4$ (see Fig. 10), one observes somewhat larger interaction of $(CH)_4$ with the allyl systems than with the pyrrole rings due to the higher amplitude of the allyl orbitals at the C_α atoms, but Fig. 10 demonstrates clearly that basically the same pattern of orbital energies is obtained. The higher symmetry causes more degeneracy, all levels except the lowest one now being doubly degenerate, in particular also the $1a_{1u}$ and $2a_{2u}$ are exactly degenerate (we retain these D_{4h} labels, although the symmetry is E_{4u} in the D_{16h} symmetry of the ring system). The configuration mixing between the excited ($1a_{1u}3e_g$ and $2a_{2u}3e_g$) configurations to form Q and B states is now a symmetry dictated formation of E_{9u} and E_{1u} states. We can thus understand that the cyclic polyene model works well. However, rather than saying that the cyclic polyene model reveals a more fundamental symmetry of the system, we would argue that the model works thanks to two factors; (1) the until now unrecognised relative inertness of the 'e_x' set of Py orbitals, effectively passivating the eight Py electrons that $(Py)_4$ has in excess over $(allyl)_4$; (2) the similar symmetry behaviour of the allyl $1a_2$ and the 'active' Py 'e_y' orbital.

The conclusion is that the similarity between the allyl $1a_2$ orbital and the 'e_y' orbital of Py explains why the cyclic polyene model (i.e. the 16-membered one) confirms to reality in the essential point of the character and (near-)degeneracy of the frontier orbitals, the $1a_{1u}$, $4a_{2u}$ pair ($\Delta = 4$ like) and the $5e_g$ pair ($\Delta = 5$ like). The prevailing feeling that the cyclic polyene model captured an essential feature of the porphin ring, and the efforts to 'save' this model in spite of disagreement with simple MO calculations, are given some justification with our fragment orbital analysis. We do not feel that the cyclic polyene model today still has a purpose as a model for explanation of the Q/B band system, in view of the problematic nature of its assumptions concerning the limited conjugation in the porphin ring system. Moreover, it is not easily extendable to chemical modifications such as fusion of benzene to the pyrrolic ring and aza substitution at the bridge positions.

5. Excited states and optical spectra

5.1. Molecular orbitals and electronic transitions

Before entering the discussion of the assignment of the electronic spectra of the systems chosen as representative of porphyrin and porphyrazine complexes, it is useful to have a general view of the transitions which may play a role in the E_u excited states which will be discussed below.

As for the porphyrin complexes, besides the nearly degenerate $\pi \rightarrow \pi^*$ transitions involving the Gouterman orbitals, the $1a_{1u} \rightarrow 5e_g$ and the $4a_{2u} \rightarrow 5e_g$, whose significance for the UV–vis spectra of porphyrins is by now well known, there are other $\pi \rightarrow \pi^*$ transitions that will contribute to the calculated E_u excited states. They are the ones out of the 'e_x'-derived set of orbitals, $2b_{2u}$, $3a_{2u}$, and $3e_g$ (cf. Figs. 2 and 4), namely the $2b_{2u} \rightarrow 5e_g$, $3a_{2u} \rightarrow 5e_g$ and $3e_g \rightarrow 2b_{1u}$. At higher energy, together with the nearly-degenerate transitions out of the Gouterman orbitals to the high lying $6e_g$ orbitals (not shown in Fig. 2), the $1a_{1u} \rightarrow 6e_g$ and the $4a_{2u} \rightarrow 6e_g$, also the transitions out of the low lying 'e_y'-derived orbitals $1b_{1u}$ (not shown in Fig. 2) and $2e_g$, namely the $2e_g \rightarrow 2b_{1u}$ and the $1b_{1u} \rightarrow 5e_g$, will enter into the excited states.

Due to the presence of 3d orbitals in the valence region, in NiP MLCT and LMCT transitions are also expected to play a role: the $d_\pi \rightarrow \pi^*$ ($4e_g \rightarrow 2b_{1u}$, $5a_{2u}$, $2a_{1u}$, $3b_{2u}$), the Np- (l.p.) $\rightarrow d\sigma^*$ ($12e_u \rightarrow 7b_{1g}$) and the $9a_{1g}(d_{z^2}) \rightarrow 13e_u$ being the only ones of E_u symmetry.

As for the porphyrazine complexes, we observe in the level diagrams of Fig. 3 as most conspicuous changes with respect to MPs (M = Mg, Zn, Ni), the stabilisation of all levels, but specially of the N_b-based $4a_{2u}$ π orbital, which is no longer degenerate with the $1a_{1u}$. In addition, three levels are introduced in the valence region that have in-plane N_b lone-pair character, namely the $6b2_g$, $12e_u$, and $8a_{1g}$. The transitions of E_u symmetry out of the N_b $6b_{2g}$ level are too high lying, however, to play a role in the excited states here considered. Therefore, the number and type of ligand centred transitions that may come into play in the E_u excited states of MPzs are the same as in MPs. With the exception of the additional N_b-(l.p.) $\rightarrow d\sigma^*$ ($12e_u \rightarrow 7b_{1g}$) LMCT transition, the number of MLCT and LMCT transitions is not expected to change going from NiP to NiPz. The differences in the orbital energies we observe on going from porphyrin to porphyrazine complexes, in particular the lifting of the $1a_{1u}/4a_{2u}$ degeneracy, are however, expected to cause substantial differences in the configuration mixings and hence in the energy and nature of the excited states.

5.2. Porphyrin complexes

Gas-phase and solution absorption spectra of square symmetric metal porphyrins are characterised by a very weak Q band in the visible showing two peaks ascribed to the (0–0) and (0–1) vibrational components, an intense feature in the near UV corresponding to the B (Soret) band, and, at the higher energy side of the Soret band, N and M bands, both attributed to the porphyrin ring [93]. Additional metal dependent L and 'extra' bands are also present in the UV region of the spectra of transition metal porphyrins. In the gas-phase spectra of Mg-Etioporphyrin (Mg-Etio) and Ni-octaethylporphyrin (NiOEP) displayed in Fig. 11 one may recognise

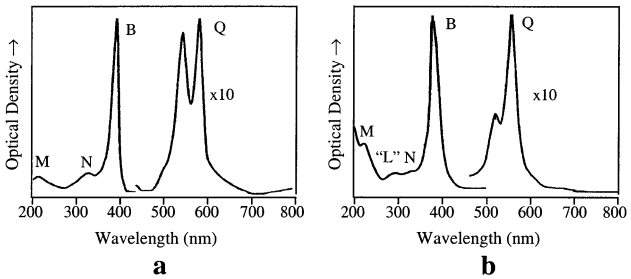

Fig. 11. Gas-phase absorption spectra of Mg–Etio (a) and NiOEP (b), from Ref. [93].

the typical features of the optical spectra of metal porphyrins.

5.2.1. Q and B bands

As inferred from Table 2 where the excitation energies and oscillator strengths calculated for the ^1E_u states of NiP and the experimental energy values determined from the CS_2 solution spectrum of NiP [86] and the gas-phase spectrum of NiOEP [93] are collected, the two lowest ^1E_u states at 2.40 and 3.23 eV beautifully account for the Q and B bands in the spectra. As a consequence of the quasi degeneracy of the $1a_{1u}$ and $4a_{2u}$ orbitals the Q and B states are a nearly 50–50 mixture of the $1a_{1u} \rightarrow 5e_g$ and $4a_{2u} \rightarrow 5e_g$ transitions. The 1^1E_u state has a very small oscillator strength (0.0052), due to opposite directions of the two large transition dipoles (the relevant dipole matrix elements are $\langle 1a_{1u} \mid y \mid 5e_{g,xz} \rangle = 3.25$ a.u., and $\langle 4a_{2u} \mid y \mid 5e_{g,yz} \rangle = 2.92$ a.u.), while the 2^1E_u where these transition dipoles are parallel has a large oscillator strength (1.02). The lowest of the allowed excitations out of the e_x-derived set of orbitals ($2b_{2u}$, $3a_{2u}$, $3e_g$) to $5e_g$ orbitals, the $2b_{2u} \rightarrow 5e_g$, is found purely in the 3^1E_u state calculated at 3.45 eV. The very small oscillator strength of this state is consistent with the poor on-site overlap between the purely $(Py)_4$-e_x $2b_{2u}$ orbital and the $(Py)_4$-e_x/π_{CH} antibonding $5e_g$, see the discussion in Section 3. Comparing to experiment, we note that the very weak 3^1E_u state will be in NiP under the high energy tail of the B band.

When comparing NiP results to TDDFT/SAOP MgP and ZnP results in Tables 3 and 4, respectively, it is apparent that in MgP and ZnP our calculations put the weak intensity $2b_{2u} \rightarrow 5e_g$ transition mostly in the 2^1E_u excited state, the Gouterman transitions entering with large weight in the much more intense and nearly degenerate 3^1E_u. On account of some Gouterman transition character, the 2^1E_u state of MgP and ZnP has, however, larger intensity than the related NiP 3^1E_u.

We assign both the 2^1E_u and 3^1E_u excited states of MgP and ZnP to the B band. This band is observed at 3.18 eV in the gas-phase spectrum of Mg-Etio, at 3.19 eV in the gas-phase spectrum of ZnOEP, and in the range 2.95–3.18 eV in the solution spectra of ZnP.

The present TDDFT/SAOP calculations for MgP excitation energies agree quite closely with the TDDFT/Becke–Perdew calculations by Sundholm [83]. Sundholm has also investigated the influence of the 1,3,5,7-tetramethyl and 2,4,6,8-tetraethyl substitutions that create the Mg-etioporphyrin, and found them to have a very small effect for the lowest excitation energy, but the substitutions may produce downward shifts of as much as 0.2–0.3 eV for higher excitation energies. At variance with TDDFT/SAOP, CASPT2 calculations on MgP [35] and TDDFT/B3LYP calculations on ZnP [43] put the $1a_{1u} \rightarrow 5e_g$ and $4a_{2u} \rightarrow 5e_g$ Gouterman transitions in the intense 2^1E_u state and the $2b_{2u} \rightarrow 5e_g$ transition

Table 2
Calculated excitation energies (eV) and oscillator strengths (f) for the optically allowed ^1E_u excited states of NiP compared with the experimental data [a]

State	Composition	Excitation energy	f	Assignment	Experimental	
					NiP [b]	NiOEP [c]
1^1E_u	50% ($1a_{1u} \rightarrow 5e_g$); 49% ($4a_{2u} \rightarrow 5e_g$)	2.40	0.0052	Q	2.28 (Q)	2.22 (Q)
2^1E_u	42%($4a_{2u} \rightarrow 5e_g$); 42%($1a_{1u} \rightarrow 5e_g$)	3.23	1.0214	B	3.11 (B)	3.22 (B)
3^1E_u	96% ($2b_{2u} \rightarrow 5e_g$)	3.45	0.0009			
4^1E_u	70% ($3a_{2u} \rightarrow 5e_g$); 29% ($4e_g \rightarrow 2b_{1u}$)	3.77	0.0294	N		3.70 (N)
5^1E_u	65% ($4e_g \rightarrow 2b_{1u}$); 26% ($3a_{2u} \rightarrow 5e_g$)	4.00	0.2526	L		4.20 (L)
6^1E_u	70% ($12e_u \rightarrow 7b_{1g}$); 9% ($4a_{2u} \rightarrow 6e_g$)	5.10	0.8960	EB_1		5.39r (EB_1)
7^1E_u	78% ($3e_g \rightarrow 2b_{1u}$); 8% ($1b_{1u} \rightarrow 5e_g$)	5.31	0.1690			
8^1E_u	62% ($1b_{1u} \rightarrow 5e_g$); 23% ($2e_g \rightarrow 2b_{1u}$); 11% ($3e_g \rightarrow 2b_{1u}$)	5.44	0.0001			
9^1E_u	87% ($4e_g \rightarrow 3b_{2u}$); 7% ($4a_{2u} \rightarrow 6e_g$)	5.64	0.2284	M		5.51 (M)
10^1E_u	38% ($4a_{2u} \rightarrow 6e_g$); 26% ($2e_g \rightarrow 2b_{1u}$); 22% ($1a_{1u} \rightarrow 6e_g$)	5.70	0.3228			

[a] The major one-electron transitions contributing to the SAOP/ALDA solution vectors are also given.
[b] CS_2 solution spectrum of NiP, from Ref. [86].
[c] Gas-phase spectrum of NiOEP, from Ref. [93].

mostly in the weak 3^1E_u state computed at quite higher energy than the 2^1E_u (0.45 eV in the CASPT2 calculations on MgP and 0.3 eV in the TDDFT/B3LYP calculations on ZnP) and consequently they assign the 2^1E_u state to the B band and the 3^1E_u state to a shoulder of the B band. Since, however, such a feature is not

Table 3
Calculated excitation energies (eV) and oscillator strengths (f) for the optically allowed ^1E_u excited states of MgP compared with experimental data

State	TDDFT/SAOP [a]				CASPT2 [b]				Experimental Mg-Etio
	Composition [c]	Excitation energy	(f)	Assignment	Composition [d]	Excitation energy	(f)	Assignment	
1^1E_u	54% ($4a_{2u} \rightarrow 5e_g$) 45% ($1a_{1u} \rightarrow 5e_g$)	2.23	0.0004	Q	39% ($4a_{2u} \rightarrow 5e_g$) 36% ($1a_{1u} \rightarrow 5e_g$)	1.66	0.004	Q	2.14 [e], 2.2 [f] (Q)
2^1E_u	77% ($2b_{2u} \rightarrow 5e_g$) 13% ($1a_{1u} \rightarrow 5e_g$) 6% ($4a_{2u} \rightarrow 5e_g$)	3.21	0.3436	B	27% ($4a_{2u} \rightarrow 5e_g$) 35% ($1a_{1u} \rightarrow 5e_g$) 6% ($3a_{2u} \rightarrow 5e_g$)	2.66	0.824	B	3.18 [e] (B)
3^1E_u	30% ($1a_{1u} \rightarrow 5e_g$) 30% ($4a_{2u} \rightarrow 5e_g$) 20% ($2b_{2u} \rightarrow 5e_g$) 17% ($3a_{2u} \rightarrow 5e_g$)	3.29	1.008		61% ($2b_{2u} \rightarrow 5e_g$)	3.11	0.150	sh	
4^1E_u	77% ($3a_{2u} \rightarrow 5e_g$) 10% ($1a_{1u} \rightarrow 5e_g$) 9% ($4a_{2u} \rightarrow 5e_g$)	3.64	0.4140	N	57% ($3a_{2u} \rightarrow 5e_g$)	3.42	0.569	N	3.81 [e] (N)
5^1E_u	93% ($3e_g \rightarrow 2b_{1u}$)	4.62	0.2546						
6^1E_u	71% ($1b_{1u} \rightarrow 5e_g$) 25% ($2e_g \rightarrow 2b_{1u}$)	5.15	0.0053						
7^1E_u	70% ($4a_{2u} \rightarrow 6e_g$) 20% ($2e_g \rightarrow 2b_{1u}$) 7% ($1a_{1u} \rightarrow 6e_g$)	5.43	0.2454	M					
8^1E_u	44% ($1a_{1u} \rightarrow 6e_g$) 24% ($4a_{2u} \rightarrow 6e_g$) 22% ($2e_g \rightarrow 2b_{1u}$)	5.59	0.0853						5.85 [e] (M)
9^1E_u	42% ($1a_{1u} \rightarrow 6e_g$) 26% ($2e_g \rightarrow 2b_{1u}$) 14% ($1b_{1u} \rightarrow 5e_g$)	5.86	0.0822						

[a] Ref. [42].
[b] Ref. [35].
[c] Major one-electron transition contributing to the SAOP/ALDA solution vectors.
[d] Main configurations of the CASSCF wave functions.
[e] Gas-phase spectrum of Mg-Etio, from Ref. [93].
[f] Low temperature matrix experiments on MgP, from Ref. [101].

Table 4
Calculated excitation energies (eV) and oscillator strengths (f) for the optically allowed ^1E_u excited states of ZnP compared with experimental data

State	TDDFT/SAOP [a]				TDDFT/B3LYP [b]				Experimental	
	Composition	Excitation energies	(f)	Assignment	Composition	Excitation energies	(f)	Assignment	ZnP	ZnOEP
1^1E_u	52% ($4a_{2u} \rightarrow 5e_g$) 47% ($1a_{1u} \rightarrow 5e_g$)	2.28	0.0019	Q	$4a_{2u} \rightarrow 5e_g$ $1a_{1u} \rightarrow 5e_g$	2.44	0.002	Q	2.03, [c] 2.21, [d] 2.23, [e] 2.18, [f] Q	2.16, [g] 2.33 [h] Q
2^1E_u	72% ($2b_{2u} \rightarrow 5e_g$) 16% ($1a_{1u} \rightarrow 5e_g$) 9% ($4a_{2u} \rightarrow 5e_g$)	3.24	0.4452	B	$4a_{2u} \rightarrow 5e_g$ $1a_{1u} \rightarrow 5e_g$	3.54	0.889	B	2.95, [c] 3.09, [d] 3.18, [e] 3.13 [f] B	3.19 [g] 3.09 [h] B
3^1E_u	32% ($4a_{2u} \rightarrow 5e_g$) 29% ($4a_{2u} \rightarrow 5e_g$) 29% ($1a_{1u} \rightarrow 5e_g$) 26% ($2b_{2u} \rightarrow 5e_g$)	3.32	1.0062		$2b_{2u} \rightarrow 5e_g$	3.84	0.052	$\pi \rightarrow \pi^*$	3.3, [d] 3.35, [e]	
4^1E_u	84% ($3a_{2u} \rightarrow 5e_g$) 6% ($1a_{1u} \rightarrow 5e_g$) 5% ($4a_{2u} \rightarrow 5e_g$)	3.66	0.5198	N	$3a_{2u} \rightarrow 5e_g$	4.29	0.175	N	4.07 [f] N	3.81 [g] 3.74 [h] N
5^1E_u	93% ($3e_g \rightarrow 2b_{1u}$)	4.61	0.2286		$4e_g \rightarrow 2b_{1u}$	5.49	0.076	L	5.18 [f] L	
6^1E_u	71% ($1b_{1u} \rightarrow 5e_g$) 26% ($2e_g \rightarrow 2b_{1u}$)	5.18	0.0044		$1b_{1u} \rightarrow 5e_g$	6.04	0.005	M		
7^1E_u	56% ($4a_{2u} \rightarrow 6e_g$) 26% ($2e_g \rightarrow 2b_{1u}$) 11% ($1a_{1u} \rightarrow 6e_g$)	5.49	0.1626		$4a_{2u} \rightarrow 6e_g$	6.40	0.023	$\pi \rightarrow \pi^*$		
8^1E_u	39% ($1a_{1u} \rightarrow 6e_g$) 37% ($4a_{2u} \rightarrow 6e_g$) 15% ($2e_g \rightarrow 2b_{1u}$)	5.64	0.0810	M					5.50 [f] M	5.97 [g] M
9^1E_u	42% ($1a_{1u} \rightarrow 6e_g$) 25% ($2e_g \rightarrow 2b_{1u}$) 14% ($1b_{1u} \rightarrow 5e_g$)	5.89	0.0646							

[a] Ref. [100].
[b] Ref. [43].
[c] Data taken in micellar solution of cetyltrimethylamonium chloride, from Ref. [102].
[d] Data taken in C_6H_6, from Ref. [103].
[e] Data taken in *n*-octane, from Ref. [104].
[f] Data taken in MeOH, from Ref.[95].
[g] Gas-phase spectrum of ZnOEP, from Ref. [93].
[h] CH_2Cl_2 spectrum of ZnOEP, from Ref. [93].

clearly identified either in the gas-phase spectrum of Mg-Etio or in the gas-phase spectrum of ZnOEP (a shoulder to the blue of the B band has been located at about 3.3 eV only in some solution spectra of ZnP), it is difficult to make a definitive assessment on the correct ordering of the 2 and 3^1E_u states of MgP and ZnP. It is clear, however, from Tables 3 and 4 that in MgP the B band is underestimated by CASPT2 calculations by $\sim$ 0.5 eV and that in ZnP the B band is overstimated by TDDFT/B3LYP calculations by $\sim$0.4 eV.

In all the investigated MPs the energies of the Q and B band are predicted at TDDFT/SAOP level in excellent accord with the experimental values, specially with the gas-phase data which even though they refer to the ethyl substituted porphyrins are still well suited for comparison with theoretical data. The relative intensities of the Q and B bands are not reproduced as well as the energies, however, the oscillator strength of the Q band being somewhat underestimated. Although this discrepancy could be due to a vibrational enhancement of the intensity of the Q band, nevertheless one should consider that the measured intensities refer to alkyl substituted metal porphyrins, while the theoretical oscillator strengths refer to the bare MPs. Calculations performed on the octamethyl substituted nickel porphyrin (NiOMP) indeed show that the alkyl substituents have the effect of increasing the intensity of the Q band for which we obtain in the NiOMP case an oscillator strength of 0.0373, a value that puts the relative intensities of the Q and B bands more in line with the experimental estimate of 1–21 [94]. In the enhancement of the intensity of the Q band on going from NiP to NiOMP one may recognise the electronic effect of the methyl groups which, by partially removing the degeneracy of the $1a_{1u}$ and $4a_{2u}$ orbitals, cause the mixing of the $1a_{1u}\rightarrow 5e_g$ and $4a_{2u}\rightarrow 5e_g$ to be less complete (the 1^1E_u state is now composed for 60% of the $1a_{1u}\rightarrow 5e_g$ and 38% of the $4a_{2u}\rightarrow 5e_g$), so there is less complete cancellation of the associated transition dipole moments. The intensities are obviously very sensitive to subtle chemical modification of the ring system.

5.2.2. N, L, M and extra bands

The number, the character and energy of the excited states accounting for the UV region change significantly on going from MgP and ZnP to NiP, MLCT and LMCT states coming into play in the latter.

According to the level diagram of Fig. 2, in NiP the excited states accounting for the UV region will involve indeed not only excitations out of the remaining orbitals of the e_x set, $3a_{2u}$, $3e_g$, out of the e_y based $2e_g$ and $1b_{1u}$, and out of the $12e_u$ N_p lone pair orbitals, but also excitations out of the metal d orbitals $9a_{1g}$ and $4e_g$.

As inferred from Table 2, the lowest allowed excitation out of the 'e_x'-derived orbitals to the $5e_g$, the $3a_{2u}\rightarrow 5e_g$, contributes with a large weight (70%) to the 4^1E_u state where it mixes to some extent with the lowest allowed MLCT transition of E_u symmetry, namely the one from the Ni-dπ $4e_g$ into the Py-e_y/π_{CH} antibonding $2b_{1u}$ orbital. The next state, 5^1E_u consists of the same transitions with ca. reversed weights to the effect that the 4^1E_u state has a prevalent $\pi\rightarrow\pi^*$ character, while the 5^1E_u state has mainly $d\pi\rightarrow\pi^*$ MLCT character. The phases of the mixing coefficients and the transition dipoles of the involved transitions are such that the 4^1E_u has quite low intensity due to opposite direction of the relatively small transition dipole matrix elements (0.95 and 0.84 a.u. for the $3a_{2u}\rightarrow 5e_g$ and $4e_g\rightarrow 2b_{1u}$, respectively), while the 5^1E_u has parallel transition dipoles and hence considerable intensity.

The assignment of the fourth and fifth singlet E_u states to the N and L bands with maxima at 3.70 eV (335 nm) and 4.20 eV (295 nm) in the absorption spectrum of NiOEP is straightforward.

It may be worthwhile mentioning that at BP level the N and L bands are predicted to have in NiP a reversed character, i.e. $d\pi\rightarrow\pi^*$ MLCT and $\pi\rightarrow\pi^*$ character, respectively. Since experimentally the L band has MLCT character, this suggests that the MLCT states are calculated at a somewhat too low energy at BP level.

In MgP and ZnP (Tables 3 and 4) we also assign the 4^1E_u state to the N band which appears at 3.81 eV (325 nm) in the gas-phase spectra of Mg-Etio and ZnOEP. This state is dominated, just as in NiP, by the $3a_{2u}\rightarrow 5e_g$ transition. The CASPT2 interpretation of the N band of MgP and the TDDFT/B3LYP interpretation of the N band of ZnP do not differ from our interpretation, although, as for the Q and B bands, the energy of the N band is underestimated at CASPT2 level and overestimated at TDDFT/B3LYP level.

The transition out of the last 'e_x' type orbital, the $3e_g$, has to go to the higher lying $2b_{1u}$ since of course excitation to $5e_g$ is forbidden by symmetry. This puts the resulting 5^1E_u states of MgP and ZnP, at 4.62 and 4.61 eV, respectively, ca. 1 eV higher than the $3a_{2u}\rightarrow 5e_g$ 4^1E_u's at 3.64 and 3.66 eV. In NiP the $3e_g\rightarrow 2b_{1u}$ is found in 7^1E_u, computed at 5.31 eV. The quite different energy of the $3e_g\rightarrow 2b_{1u}$ $7^1E_u$of NiP is well accounted for by the $3e_g$ being strongly stabilised in NiP (see Fig. 2) by bonding interaction with Ni-$3d_\pi$ orbitals.

Comparing to experiment, we note that the 5^1E_u state will be in MgP and in ZnP under the broad high energy tail of the N band. The 5^1E_u state of ZnP is computed at TDDFT/B3LYP level at much higher energy than at TDDFT/SAOP level (5.49 vs. 4.61 eV) and is assigned to a band denoted as L appearing in the MeOH solution spectrum of ZnP at 5.18 eV [95].

The description of the N band of MPs as $\pi\rightarrow\pi^*$ and of the L band of NiP as MLCT that emerges from TDDFT/SAOP calculations nicely explains why the N band appears quite constant in the vapour phase spectra of metal-porphyrins, and the L band, which is observed

only in transition metal porphyrins with incomplete d shell, varies considerably with the metal in both energy and intensity.

As for the higher excited states, in NiP a quite large energy gap (1.1 eV) separates the 5^1E_u corresponding to the L band from the set of the remaining ^1E_u states describing the UV region of the spectrum. This region is characterised by the M band centred at 5.51 eV (225 nm) which actually appears as a pronounced shoulder of the EB_1 'extra' band starting at 5.39 eV (230 nm) and extending below 200 nm (see Fig. 11b).

As shown in Table 2, in this region we find excited states with $\pi \rightarrow \pi^*$ character, such as the 7, 8, and 10^1E_u, interspersed with excited states with LMCT/MLCT character, such as the 6 and 9^1E_u. This fits in with the M band which is characteristic of the porphyrin ring and the metal-dependent EB_1 'extra' band being strongly overlapped. The energy of the lowest state of this set, the 6^1E_u, which is mainly a $n \rightarrow d\sigma^*$ state as it involves the low lying $12e_u$ N_p lone pair orbital and the Ni $d_{x^2-y^2}$ orbital and which is characterised by a large transition moment (1.73 a.u., the largest after the Gouterman transitions), appears to be underestimated by our calculations. This state is indeed expected to contribute to the intense part of the metal-dependent EB_1 'extra' band at higher energy than the M shoulder, while it is calculated to the red of the M band. The energy, intensity and character of the M band in NiP are well accounted for by the 9^1E_u (MLCT) and 10^1E_u ($\pi \rightarrow \pi^*$) excited states calculated at 5.64 and 5.70 eV with oscillator strengths of 0.2284 and 0.3228.

In MgP and ZnP the M band region is not complicated by MLCT and LMCT states and the assignment of this band is more straightforward than in NiP. As inferred from Tables 3 and 4, for the assignment of the M band of MgP and ZnP, the 7^1E_u state is the best candidate. Comparison with the band maxima of 5.85 and 5.97 eV obtained from gas-phase spectra of Mg-Etio and ZnOEP, respectively, suggests that our TDDFT/SAOP calculations slightly underestimate the energy of the M band, although the 5.50 eV for ZnP in MeOH solution is in agreement with the calculated energy of 5.49 eV of the 7^1E_u. It should also be noted that the 7^1E_u contributes only 50% to the intensity of the M band, the remaining 50% coming from the two next excited states, the 8 and 9^1E_u computed at 5.59 and 5.86 eV in MgP and at 5.64 and 5.89 eV in ZnP, which puts our results more in line with the experiment. It is worth noting that the composition of the 7^1E_u excited state of MgP and ZnP is nearly identical to that of the 10^1E_u ($\pi \rightarrow \pi^*$) excited state contributing to the M band in NiP.

5.3. Porphyrazine complexes

Due to a rather complex synthetic pathway and to the low solubility, porphyrazines have received relatively little attention compared with porphyrins. Although the discovery of efficient synthetic routes has recently disclosed the potential of this class of tetrapyrroles [96], the study of their physico-chemical properties is still at its infancy. As for the optical spectra, gas-phase spectra of porphyrazines have not been reported so far and the solution spectra available have been generally taken in strongly coordinating solvents, and cover a rather narrow energy range (2.1–4.1 eV) [4]. The nickel, magnesium and zinc porphyrazine complexes, which are here considered, do not represent an exception in this respect.

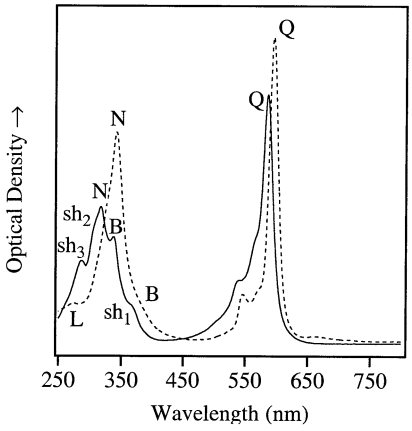

Fig. 12. Absorption spectra of MgOEPz (-----) and NiOEPz (—) in hexane at room temperature (r.t.), from Ref. [40].

In order to have experimental data more suitable for comparison, we have recently collected the optical spectra of MgOEPz (OEPz = octaethylporphyrazine) and of the newly synthesised NiOEPz, in a diluted solution of a noncoordinating solvent, hexane, in the range 1.5–5.0 eV [40]. The spectra are displayed in Fig. 12. The solution spectrum reported by Dvornikov et al. [91] for ZnPz, in the range 2.0–4.1 eV, does not differ substantially from the spectrum of MgOEPz of Fig. 12 except for a more pronounced breadth of near-UV features, most likely due to solvent effects.

The visible region is dominated by an intense Q band showing vibrational structure and centred at 2.11 eV (590 nm) in NiOEPz, 2.08 eV (596 nm) in MgOEPz, 2.13 eV (582 nm) in ZnPz. Note that the Q band is not multiplied by a factor 10 as in the case of the porphyrin complexes in Fig. 11. The near UV region is somewhat different in NiOEPZ compared with MgOEPz and ZnPz. In NiOEPz it is characterised by a broad and structured band beginning at ~3.0 eV (413 nm) and extending at least 2.0 eV to higher energy. It shows a weak shoulder, sh_1, at 3.30 eV (376 nm), a pronounced shoulder at 3.65 eV (340 nm) denoted according to the nomenclature used by Weiss et al. [14] as B, a main peak centred at 3.91 eV (317 nm) denoted by Weiss et al. [14] as N, and two shoulders, sh_2 and sh_3, at 4.0 eV (310 nm) and 4.29 eV (289 nm), respectively.

In MgOEPz and specially in ZnPz the broad band in the near UV is much less structured than in NiOEPz and slightly red shifted.

The excitation energies and oscillator strengths calculated for the ^1E_u states of NiPz up to 5.0 eV and the experimental energy values determined from the solution spectrum of NiOEPz are gathered in Table 5.

The lifting of the (near-)degeneracy of the $1a_{1u}$ and $4a_{2u}$ orbitals in NiPz causes the $1a_{1u} \rightarrow 5e_g$ and $4a_{2u} \rightarrow 5e_g$ one-electron transitions to mix very little. This has important consequences for the nature and intensity of the lowest excited states. The 1^1E_u excited state is mainly (84%) described by the $1a_{1u} \rightarrow 5e_g$ transition, the $4a_{2u} \rightarrow 5e_g$ entering with only a minor weight (14%). The cancellation of the transition dipoles of the $1a_{1u} \rightarrow 5e_g$ and $4a_{2u} \rightarrow 5e_g$ configurations that occurs in the lowest excited state in porphyrins, leading to very low intensity of the Q bands, occurs to a much lesser extent in NiPz, leading, in agreement with experiment, to an intense Q band ($f = 0.2692$). The $2b_{2u} \rightarrow 5e_g$ and the $3a_{2u} \rightarrow 5e_g$ configurations occur almost purely in the weak 2 and 3^1E_u excited states, respectively, at lower energy than the second Gouterman transition, the $4a_{2u} \rightarrow 5e_g$ (which mixes with some $1a_{1u} \rightarrow 5e_g$ and other configurations, vide infra). The low intensity of the 2 and 3^1E_u states fits in with the 'e_x' character of the $2b_{2u}$ and $3a_{2u}$ orbitals. We note that the small change in composition of these orbitals due to the aza substitution in the ring, now makes the $2b_{2u} \rightarrow 5e_g$ the more intense one of the two, leaving virtually zero transition dipole matrix element for the $3a_{2u} \rightarrow 5e_g$, just opposite to the situation in NiP. We assign the 2 and 3^1E_u states to the shoulder sh_1 at 3.30 eV.

Due to the downward shift of the $4a_{2u}$, the high energy combination of the $4a_{2u} \rightarrow 5e_g$ and $1a_{1u} \rightarrow 5e_g$ excited configurations undergoes further configuration interaction with the nearly degenerate $4e_g \rightarrow 2b_{1u}$ $d_\pi \rightarrow \pi^*$ and the $12e_u \rightarrow 7b_{1g}$ $N_b(l.p.) \rightarrow d\sigma^*$ excitations. (What we call 'the high energy combination of the $4a_{2u} \rightarrow 5e_g$ and $1a_{1u} \rightarrow 5e_g$', to stress the analogy with porphyrins, has actually rather little weight of $1a_{1u} \rightarrow 5e_g$, the lifting of the $1a_{1u}/4a_{2u}$ degeneracy in the porphyrazine suppressing the mixing of the Gouterman transitions to a large extent.) It should be noted that, due to its bridge lone pair character, the $12e_u$ is in NiPz at much higher energy than the $N_p(l.p.)$ $12e_u$ in NiP (see Figs. 2 and 3). Three excited states result from this configurational mixing, the 4, 5, and 6^1E_u calculated at 3.51, 3.67 and 3.89 eV, respectively. As for the states, which contain the high energy combination of the $4a_{2u} \rightarrow 5e_g$ and $1a_{1u} \rightarrow 5e_g$ excited configurations, namely the 4 and 6^1E_u, the phases of the mixing coefficients and the transition dipoles of the involved transitions are such that the 4^1E_u has much lower intensity ($f = 0.1465$) than the 6^1E_u ($f = 0.9220$). According to their energy and oscillator strength, the 4 and 6^1E_u excited states are responsible for the B and N bands, respectively.

In the region between 3.89 and 5.8 eV we find only a weak excited state at 5.15 eV, the 7^1E_u, which is mainly described by the $3e_g \rightarrow 2b_{1u}$ $\pi \rightarrow \pi^*$ transition. Since we do not believe our calculations can be so much in error, the shoulders to the blue of the most intense UV peak, sh_2 at 4.0 eV (310 nm) and sh_3 at 4.29 eV (289 nm) should be vibrational in origin.

It should be noted that the character of the B and N bands of NiPz is very different from the character predicted by Weiss et al. [14] for these bands in the case of MgOMPz (OMPz = octamethylporphyrazine), the B and N states of NiPz involving to a large extent MLCT and LMCT transitions. The observed sensitivity to the metal of the energy and intensity of the B and N bands in transition metal porphyrazines, not observed in metal porphyrins, [93] suggests that the presence of MLCT and LMCT transitions in the B–N region is not a peculiarity of the nickel porphyrazine.

Athough the B and N bands have a different nature in transition metal porphyrazines compared with alkaline-earth metal and zinc porphyrazines, nevertheless they originate by the same mechanism. This is in essence the mixing of the high energy combination of the $^1(4a_{2u}5e_g)$

Table 5
Calculated excitation energies (eV) and oscillator strengths (f) for the optically allowed ^1E_u excited states of NiPz compared with the experimental data [a]

State	Composition	Excitation energies	f	Assignment	Experimental
					NiOEPz [b]
1^1E_u	84% ($1a_{1u} \rightarrow 5e_g$); 14% ($4a_{2u} \rightarrow 5e_g$)	2.42	0.2692	Q	2.11
2^1E_u	97%($2b_{2u} \rightarrow 5e_g$)	3.00	0.0226	sh_1	3.30
3^1E_u	85% ($3a_{2u} \rightarrow 5e_g$); 9% ($4e_g \rightarrow 2b_{1u}$)	3.38	0.00002		
4^1E_u	44% ($4e_g \rightarrow 2b_{1u}$); 38% ($4a_{2u} \rightarrow 5e_g$); 14% ($12e_u \rightarrow 7b_{1g}$); 3% ($1a_{1u} \rightarrow 5e_g$)	3.51	0.1465	B	3.65
5^1E_u	61% ($12e_u \rightarrow 7b_{1g}$); 28% ($4e_g \rightarrow 2b_{1u}$)	3.67	0.0300		
6^1E_u	38% ($4a_{2u} \rightarrow 5e_g$); 22% ($12e_u \rightarrow 7b_{1g}$); 17% ($4e_g \rightarrow 2b_{1u}$); 8% ($1a_{1u} \rightarrow 5e_g$)	3.89	0.9220	N	3.91
7^1E_u	96% ($3e_g \rightarrow 2b_{1u}$)	5.15	0.0051		

[a] Ref. [40]. The major one-electron transitions contributing to the SAOP/ALDA soluction vectors are also given.
[b] Hexane solution spectrum of NiOEPz, from Ref. [40].

and $^1(1a_{1u}5e_g)$ excited configurations, which is actually mostly $^1(4a_{2u}5e_g)$ and is raised in energy by the downward shift of the $4a_{2u}$, with the closest lying available configurations, which are of MLCT ($4e_g \rightarrow 2b_{1u}$) and LMCT ($12e_u \rightarrow 7b_{1g}$) type in nickel and presumably in other transition metal porphyrazines, and of $\pi \rightarrow \pi^*$ type in magnesium, zinc and FBPz.

SCMO PPP results on MgOMPz [14] and our results on NiPz already point to this mechanism, but a definitive assessment comes from TDDFT calculations of the excited states of MgPz and ZnPz.

In Tables 6 and 7 the excitation energies and oscillator strengths calculated for the ^1E_u states of MgPz and ZnPz, respectively, are reported and compared with the experimental data. According to our TDDFT/SAOP results, the 3 and 4^1E_u excited states calculated at 3.08 and 3.74 eV in MgPz and at 3.16 and 3.69 in ZnPz are responsible for the B and N bands appearing in the spectrum of MgOEPz at 3.31 eV (402 nm) and 3.61 eV (332 nm) and in the spectrum of ZnPz at 3.44 eV (360 nm) and at 3.73 eV (332 nm) are a mixture of the high energy combination of the $^1(4a_{2u}5e_g)$ and $^1(1a_{1u}5e_g)$ excited configurations with the $^1(3a_{2u}5e_g)$ $\pi \rightarrow \pi^*$ configuration. One may wonder why the $^1(3a_{2u}5e_g)$ $\pi \rightarrow \pi^*$ configuration mixes with the $^1(4a_{2u}5e_g)$ and $^1(1a_{1u}5e_g)$ excited configurations in MgPz and in ZnPz but not in NiPz. The reason is that in MgPz and ZnPz, owing to the ring deformation caused by the increased hole size of the macrocycle (the $M-N_p$ distance is 1.998 Å in MgPz, 1.981 Å in ZnPz, 1.894 Å in NiPz), the $4a_{2u}$ is pushed up compared with NiPz (see Fig. 3). As a consequence the high energy combination of the $^1(4a_{2u}5e_g)$ and $^1(1a_{1u}5e_g)$ excited configurations is in MgPz and ZnPz at lower energy than in NiPz and hence more suitable for interaction with the $^1(3a_{2u}5e_g)$ configuration. The shift to lower energy of the high energy combination of the $^1(4a_{2u}5e_g)$ and $^1(1a_{1u}5e_g)$ excited configurations on going from NiPz to ZnPz and MgPz is just at the origin of the red shift of the B–N system in MgPz and ZnPz.

The progressive rise in energy of the $4a_{2u}$ level on going from NiPz to ZnPz and MgPz also causes the mixing of the Gouterman's excited configurations in the 1^1E_u excited state to increase in the same direction, as inferred from the composition of this state reported in Tables 5–7.

A few other points are worth mentioning concerning the excited states of MPzs. In MgPz and ZnPz the lowest excitation out of the 'e_x'-derived set of orbitals to $5e_g$ orbitals, the $2b_{2u} \rightarrow 5e_g$, is found to not mix at all with other configurations, at variance with SCMO PPP results [14], but in line with TDDFT/SAOP results on NiPz, NiP, MgP, and ZnP as well as with TDDFT/B3LYP results on ZnP and ZnPz [43], and CASPT2 results on MgP [35]. This transition is buried under the B band in MgPz and ZnPz, while it results in a distinguishable shoulder, sh_1, of the B band in NiPz.

As inferred from Table 7, our TDDFT/SAOP calculations and TDDFT/B3LYP calculations by Nguyen and Pachter [43] provide substantially the same qualitative interpretation of the ZnPz spectrum, apart from the use of a different notation of the near UV bands, which are indeed denoted by these authors as B_1 and B_2 (in analogy with phthalocyanines), rather than B and N. The TDDFT/B3LYP excitation energies are, however, too high compared with the experimental values, so the TDDFT/B3LYP calculations seem to have a tendency to overestimate the excitation energies of tetrapyrrole complexes. This behaviour of the TDDFT/B3LYP calculations also emerges in TDDFT/B3LYP excitations on the zinc phthalocyanine complex [43], which nicely agree with experiment and with TDDFT/SAOP calculations on the same complex [41] for the Q band, but are typically 0.5–0.6 eV higher for the subsequent excitations. Detailed comparison with experiment, including MCD spectra, has provided confidence in the TDDFT/SAOP results [98].

As for the states to the blue of the N band, we note that the $3e_g \rightarrow 2b_{1u}$ transition that in NiPz is found almost purely in the high lying, very weak 7^1E_u excited state, in MgPz and ZnPz is found to dominate a state, the 5^1E_u, that is much lower lying and much more intense than the 7^1E_u state of NiPz, as it is calculated in MgPz at 4.36 eV with an oscillator strength of 0.2290, and in ZnPz at 4.27 eV with an oscillator strength of

Table 6
Calculated excitation energies (eV) and oscillator strengths (f) for the optically allowed ^1E_u excited states of MgPz compared with the experimental data [a]

State	Composition	Excitation energies	(f)	Assignment	Experimental
					MgOEPz [b]
1^1E_u	74% ($1a_{1u} \rightarrow 5e_g$); 22% ($4a_{2u} \rightarrow 5e_g$)	2.34	0.2308	Q	2.08
2^1E_u	97% ($2b_{2u} \rightarrow 5e_g$)	2.81	0.0235		
3^1E_u	58% ($3a_{2u} \rightarrow 5e_g$); 37% ($4a_{2u} \rightarrow 5e_g$); 4% ($1a_{1u} \rightarrow 5e_g$)	3.08	0.0540	B	3.31
4^1E_u	39% ($4a_{2u} \rightarrow 5e_g$); 35% ($3a_{2u} \rightarrow 5e_g$); 19% ($1a_{1u} \rightarrow 5e_g$)	3.74	1.7084	N	3.61
5^1E_u	92% ($3e_g \rightarrow 2b_{1u}$)	4.36	0.2290	L	4.52

[a] Ref. [40]. The major one-electron transitions contributing to the SAOP/ALDA soluction vectors are also given.
[b] Hexane solution spectrum of MgOEPz, from Ref. [40].

Table 7
Calculated excitation energies (eV) and oscillator strengths (f) for the optically allowed ^1E_u excited states of ZnPz compared with experimental data

State	TDDFT/SAOP [a]				TDDFT/B3LYP [b]				Experimental
	Composition	Excitation energies	(f)	Assignment	Composition	Excitation energies	(f)	Assignment	
1^1E_u	78% ($1a_{1u} \rightarrow 5e_g$) 19% ($4a_{2u} \rightarrow 5e_g$)	2.34	0.2530	Q	$1a_{1u} \rightarrow 5e_g$	2.48	0.148	Q	2.13 [c]
2^1E_u	97% ($2b_{2u} \rightarrow 5e_g$)	2.81	0.0238		$2b_{2u} \rightarrow 5e_g$	3.38	0.018	$\pi \rightarrow \pi^*$	
3^1E_u	75% ($3a_{2u} \rightarrow 5e_g$) 21% ($4a_{2u} \rightarrow 5e_g$)	3.16	0.0135	B	$3a_{2u} \rightarrow 5e_g$	3.78	0.114	B_1	3.44 [c]
4^1E_u	56% ($4a_{2u} \rightarrow 5e_g$) 19% ($3a_{2u} \rightarrow 5e_g$) 17% ($1a_{1u} \rightarrow 5e_g$)	3.69	1.456	N	$3a_{2u} \rightarrow 5e_g$ $4a_{2u} \rightarrow 5e_g$	4.04	0.714	B_2	3.73 [c]
5^1E_u	92% ($3e_g \rightarrow 2b_{1u}$)	4.27	0.2204	L	$4e_g \rightarrow 2b_{1u}$	5.20	0.055	L	

[a] Ref. [100].
[b] Ref. [43].
[c] Ref. [97].

0.2204. We assign the 5^1E_u states of MgPz and ZnPz to the L band. This band appears in the spectrum of MgOEPz to the blue of the N band, at 4.52 eV (274 nm), but not in the spectrum of ZnPz which is recorded in a too small energy range for the L band to be visible, although it is reasonable to assume that in ZnPz the L band is located at ca. the same energy as in MgPz. That the 5^1E_u states of MgPz and ZnPz have so different energy and intensity compared with the 7^1E_u state of NiPz, although they are all dominated by the $3e_g \rightarrow 2b_{1u}$ transition, is understandable in the light of the different composition and energy of the 'e_x'-derived $3e_g$ orbital in the three complexes. In MgPz and ZnPz the $3e_g$ is a pure 'e_x'-derived Pz orbital with large amplitude on N_p (35%) and C_α (57%) atoms, whereas in NiPz the $3e_g$ is pushed to lower energy by the $3d_\pi$–$4e_g$ and acquires a 29% of metallic character at the expense of the C_α (46%) character. The decreased C_α amplitude sensibly reduces the on site overlap with the $2b_{1u}$, the resulting transition dipole matrix element of the $3e_g \rightarrow 2b_{1u}$ being in NiPz half of that in MgPz and ZnPz (0.32 vs. 0.69 and 0.70 a.u.).

Finally, we would like to make some comments on the intensities of the main features of the electronic spectra of MPzs.

The relative intensities of the Q, B and N bands (cf. the relative heights of the bands in Fig. 12) do not seem to be well reproduced by our calculations. The stronger intensity of the N band than the B band, in particular in MgPz, is correctly reproduced, but we calculate a rather low oscillator strength for the Q band as compared with the N band. This does not necessarily mean, however, that the calculated oscillator strengths are incorrect. As shown by Gouterman in the case of free base and zinc–phthalocyanines [16], one should not compare calculated oscillator strengths to measured maximum extinction coefficients (ε_{max}), but, more realistically, to the experimental oscillator strengths which are ca. proportional to the maximum extinction coefficients times the half-bandwidth, $\Delta_{1/2}$ ($f \propto \varepsilon_{max}\,\Delta_{1/2}$). Given the considerable broadening of the B–N system in MgOEPz, ZnPz and NiOEPz, it is likely that the experimental oscillator strengths of the B, N and Q bands, if available, would better agree with the calculated oscillator strengths than the maximum extinction coefficients do. Of course, one should keep in mind that the calculated oscillator strengths do not include vibrational coupling effects.

We also have to take into account that the calculations obviously deviate in several respects from the experimental situation. Solvent effects, which are not considered in our calculations, could influence the relative intensities of these bands, as suggested by the observed pronounced sensitivity to the solvent of the intensity and often of the energy of the main bands in metal-porphyrazines [99]. The effect of the substituents is important as well, as found in the case of NiP. Our calculations predict indeed an increase of the oscillator strength of the Q state going from NiPz to the methyl substituted nickel-porphyrazine.

6. Summary

The ground state electronic structure of MgP, ZnP, NiP, MgPz, ZnPz, and NiPz systems, taken as representative of nontransition and transition metal porphyrin and porphyrazine complexes, is highlighted using a fragment approach with the four pyrrole rings and the methine or aza bridges as building blocks. It is elucidated how the time-honoured explanation of the intensity distribution in the Q and B bands from a simple polyene model can be reconciled with the actual structure of the ring systems being much more complicated. The crucial point is that the special orbital structure of the pyrrole units affords a simplification to simple allylic units, which would generate together

with the methine bridges, a pure cyclic polyene. However, the full complexity of the spectra, which feature additional shoulders and bands, the details of the intensity patterns, and the effect of tetraaza substitution, can only be understood by taking into account the full orbital structure of the pyrrole, as well as the electronic difference between methine and aza bridges. The electronic structure analysis given provides a basis for the interpretation of the time-dependent density functional calculations of the excited states of investigated porphyrin and porphyrazine complexes.

The TDDFT/SAOP results prove to agree very well with the experimental data. Comparing with TDDFT/B3LYP calculations for the Zn complexes [43]it is to be noted that for the Q band there is good agreement, but for the higher excitations the TDDFT/B3LYP model appears to consistently obtain higher excitation energies than the TDDFT/SAOP model. Comparing with experiment, the TDDFT/B3LYP excitation energies often appear to be somewhat too high, while TDDFT/SAOP, if anything is at the low side. The differences do not lead to major discrepancies in the assignments of the electronic structure origins of the experimental bands, although there are differences in the details for the higher excitations. In the case of Zn phthalocyanine, where detailed experimental results are available, the same pattern of too high excitation energies for TDDFT/B3LYP seems to exist [41,43]. Further investigation on model transition metal complexes with unambiguously assigned spectra seems to be in order.

The results for assignments of the UV–vis spectra of the title compounds may be summarised as follows:

1) In porphyrins the proximity of the $1a_{1u}$ and $4a_{2u}$ orbitals causes the (near)-degenerate ($1a_{1u}5e_g$) and ($4a_{2u}5e_g$) configurations to strongly mix in the 1 and 2^1E_u (or 3^1E_u) excited states. The phases of the mixing coefficients and transition dipoles are such that the low energy combination occurring in the 1^1E_u state responsible for the Q band has low intensity, due to opposite directions of the two large transition dipoles, while the high energy combination occurring in the 2^1E_u (or 3^1E_u) state responsible for the B band has parallel transition dipoles and therefore, high intensity.The lifting of the (near)-degeneracy of the a_{1u} and a_{2u} Gouterman orbitals in porphyrazines causes the mixing between the ($1a_{1u}5e_g$) and ($4a_{2u}5e_g$) configurations to decrease considerably. The cancellation of transition dipoles that occurs in the low energy combination of the Gouterman configurations in porphyrins, leading to very low intensity of the Q bands, occurs to a much smaller degree in porphyrazines.
2) The breakdown of the (near)-degeneracy of the Gouterman configurations also causes the B band of the magnesium and nickel porphyrazines to be different in origin from the B band of their porphyrin analogs.The high energy combination of the ($1a_{1u}5e_g$) and ($4a_{2u}5e_g$) configurations that is at the origin of the B band in metal porphyrins, loses indeed to a large extent the contribution of the ($1a_{1u}5e_g$) configuration, and moreover mixes with other configurations which are of MLCT ($4e_g \rightarrow 2b_{1u}$) and LMCT ($12e_u \rightarrow 7b_{1g}$) type in nickel and presumably in other transition metal porphyrazines, and of $\pi \rightarrow \pi^*$ type ($3a_{2u} \rightarrow 5e_g$) in magnesium, zinc and FBPz.
3) Although the introduction of the 3d levels does not make radical changes in the absorption spectra, the $d \rightarrow d$ transitions being parity forbidden, the remarkable sensitivity to the metal of some features of the spectra fits in with the MLCT $d_\pi \rightarrow \pi^*$ and the LMCT N(l.p.) $\rightarrow d\sigma^*$ (either N_b-(l.p.) or N_p-(l.p.)) transitions coming into play in transition metal porphyrins and porphyrazines. As a matter of fact, in NiP the L band has mainly $d_\pi \rightarrow \pi^*$ MLCT character, the N_p(l.p.) $\rightarrow d\sigma^*$ LMCT transitions appearing at higher energy, namely in the region of the M and EB_1 bands.In NiPz, where the B band occurs at higher energy than in NiP, the low lying N_b (l.p.) $\rightarrow d\sigma^*$ LMCT transition comes into play already in the B band region, and the $d_\pi \rightarrow \pi^*$ MLCT transition contributes to the B–N band system.

Acknowledgements

We are pleased to acknowledge Professor Dick Stufkens for exciting our interest in the excitation spectra and photochemistry of transition metal complexes and for the many stimulating discussions. We thank the Italian MURST (Ministero dell' Università e della Ricerca Scientifica) and the Università della Basilicata, Italy (GRANT 9903263473_005), and the National Computing Facilities Foundation (NCF) of the Netherlands Foundation for Scientific Research (NWO) for a grant of computer time.

References

[1] D. Dolphin (Ed.), The Porphyrins, vol., Academic Press, New York, 1978–1979, p. Pages.
[2] R.W. Wagner, J.S. Lindsey, J. Seth, V. Palaniappan, D.F. Bocian, J. Am. Chem. Soc. 118 (1996) 3996.
[3] J.R. Reimers, T.X. Lü, M.J. Crossley, N.S. Hush, Chem. Phys. Lett. 256 (1996) 353.
[4] C.C. Leznoff, A.B.P. Lever (Eds.), Phthalocyanines: Properties and Applications, vol. 1–4, VCH Publishers, New York, 1990–1996, p. Pages.
[5] S. Pryadarshy, M.J. Therien, D.N. Beratan, J. Am. Chem. Soc. 118 (1996) 1504.

[6] D. Beljonne, G.E. O'Keefe, P.J. Hamer, R.H. Friend, H.L. Anderson, J.L. Brédas, J. Chem. Phys. 106 (1997) 9439.
[7] F.Z. Henari, W.J. Blau, L.R. Milgrom, G. Yahioglu, D. Phillips, J.A. Lacey, Chem. Phys. Lett. 267 (1997) 229.
[8] Z. Wang, P.N. Day, R. Pachter, J. Chem. Phys. 108 (1998) 2504.
[9] P. Chen, I.V. Tomov, A.S. Dvornikov, M. Nakashima, J.F. Roach, D.M. Alabram, P.M. Rentzepis, J. Phys. Chem. 100 (1996) 17507.
[10] P. Sayer, M. Gouterman, C.R. Connell, Acc. Chem. Res. 15 (1982) 73.
[11] C. Weiss, J. Mol. Spectrosc. 44 (1972) 37.
[12] L. Edwards, M. Gouterman, J. Mol. Spectrosc. 33 (1970) 292.
[13] L. Bajema, M. Gouterman, C.B. Rose, J. Mol. Spectrosc. 39 (1971) 421.
[14] C. Weiss, H. Kobayashi, M. Gouterman, J. Mol. Spectrosc. 16 (1965) 415.
[15] M. Gouterman, J. Chem. Phys. 30 (1959) 1139.
[16] M. Gouterman, J. Mol. Spectrosc. 6 (1961) 138.
[17] M. Gouterman, G. Wagnière, L.C. Snyder, J. Mol. Spectrosc. 11 (1963) 108.
[18] W.T. Simpson, J. Chem. Phys. 17 (1949) 1218.
[19] J.R. Platt, in: A. Hollaender (Ed.), Radiation Biology, vol. 3, McGraw Hill, New York, 1956, pp. 71–123.
[20] I. Baraldi, A. Carnevali, G. Ponterini, D. Vanossi, J. Mol. Struct.: Theochem 333 (1995) 121.
[21] M.J. Stillman, in: C.C. Leznoff, A.B.P. Lever (Eds.), Phthalocyanines: Properties and Applications, vol. III (Chapter 5), VCH Publishers, New York, 1993, pp. 227–296.
[22] B.H. Huynh, D.A. Case, M. Karplus, J. Am. Chem. Soc. 99 (1977) 6013.
[23] D.H. Jones, A.S. Hinman, T. Ziegler, Inorg. Chem. 32 (1993) 2092.
[24] S.F. Sontum, D.A. Case, M. Karplus, J. Chem. Phys. 79 (1983) 2881.
[25] X.L. Liang, S. Flores, D.E. Ellis, B.M. Hoffman, R.L. Musselman, J. Chem. Phys. 95 (1991) 403.
[26] L. Guo, D.E. Ellis, B.M. Hoffman, Y. Ishikawa, Inorg. Chem. 35 (1996) 5304.
[27] M. Merchán, E. Ortí, B.O. Roos, Chem. Phys. Lett. 226 (1994) 27.
[28] H. Nakatsuji, J. Hasegawa, M. Hada, J. Chem. Phys. 104 (1996) 2321.
[29] M. Nooijen, R.J. Bartlett, J. Chem. Phys. 106 (1997) 6449.
[30] S.R. Gwaltney, R.J. Bartlett, J. Chem. Phys. 108 (1998) 6790.
[31] Y. Tokita, J. Hasegawa, H. Nakatsuji, J. Phys. Chem. A102 (1998) 1843.
[32] L. Serrano-Andrés, M. Merchán, M. Rubio, B.O. Roos, Chem. Phys. Lett. 295 (1998) 195.
[33] T. Hashimoto, Y.-K. Choe, H. Nakano, K. Hirao, J. Phys. Chem. A 103 (1999) 1894.
[34] J. Hasegawa, M. Hada, M. Nonoguchi, H. Nakatsuji, Chem. Phys. Lett. 250 (1996) 159.
[35] M. Rubio, B.O. Roos, L. Serrano-Andrés, M. Merchán, J. Chem. Phys. 15 (1999) 7202.
[36] S.J.A. van Gisbergen, A. Rosa, G. Ricciardi, E.J. Baerends, J. Chem. Phys. 111 (1999) 2505.
[37] D. Sundholm, Chem. Phys. Lett. 302 (1999) 480.
[38] D. Sundholm, Phys. Chem. Chem. Phys. 2 (2000) 2275.
[39] G. Ricciardi, A. Rosa, S.J.A. van Gisbergen, E.J. Baerends, J. Phys. Chem. A 104 (2000) 635.
[40] A. Rosa, G. Ricciardi, E.J. Baerends, S.J.A. van Gisbergen, J. Phys. Chem. A 105 (2001) 3311.
[41] G. Ricciardi, A. Rosa, E.J. Baerends, J. Phys. Chem. A 105 (2001) 3340.
[42] A. Rosa, G. Ricciardi, E.J. Baerends, S.J.A. van Gisbergen, Eighth International Conference on the Applications of Density Functional Theory to Chemistry and Physics, Rome, Italy, 1999 p. 38.
[43] K.A. Nguyen, R. Pachter, J. Chem. Phys. 114 (2001) 10757.
[44] A.B.J. Parusel, S. Grimme, J. Porphyrins Phthalocyanines 5 (2001) 225.
[45] E.J. Baerends, O.V. Gritsenko, R. van Leeuwen, in: B.B. Laird, R.B. Ross, T. Ziegler (Eds.), Chemical Applications of Density Functional Theory, vol. 629, American Chemical Society, Washington, DC, 1996, pp. 20–41.
[46] E.J. Baerends, O.V. Gritsenko, J. Phys. Chem. A101 (1997) 5383.
[47] O.V. Gritsenko, R. van Leeuwen, E.J. Baerends, J. Chem. Phys. 101 (1994) 8955.
[48] P. Süle, O.V. Gritsenko, A. Nagy, E.J. Baerends, J. Chem. Phys. 103 (1995) 10085.
[49] F.M. Bickelhaupt, E.J. Baerends, in: K.B. Lipkowitz, D.R. Boyd (Eds.), Reviews in Computational Chemistry, vol. 15, Wiley, New York, 2000, pp. 1–86.
[50] E.J. Baerends, D.E. Ellis, P. Ros, Chem. Phys. 2 (1973) 41.
[51] G. te Velde, E.J. Baerends, J. Comp. Phys. 99 (1992) 84.
[52] C. Fonseca Guerra, J.G. Snijders, G. te Velde, E.J. Baerends, Theo. Chem. Acc. 99 (1998) 39.
[53] O.V. Gritsenko, P.R.T. Schipper, E.J. Baerends, Chem. Phys. Lett. 302 (1999) 199.
[54] P.R.T. Schipper, O.V. Gritsenko, S.J.A. van Isbergen, E.J. Baerends, J. Chem. Phys. 112 (2000) 1344.
[55] A. Becke, Phys. Rev. A38 (1988) 3098.
[56] J.P. Perdew, Phys. Rev. B 33 (1986) 8822 (Erratum: PRB 34 (1986) 7406).
[57] A. Zangwill, P. Soven, Phys. Rev. 21 (1980) 1561.
[58] M.J. Stott, E. Zaremba, Phys. Rev. 21 (1980) 12.
[59] G.D. Mahan, Phys. Rev. A22 (1980) 1780.
[60] B.M. Deb, S.K. Ghosh, Int. J. Quantum Chem. 23 (1983) 1.
[61] E. Runge, E.K.U. Gross, Phys. Rev. Lett. 52 (1984) 997.
[62] E.K.U. Gross, W. Kohn, Adv. Quantum Chem. 21 (1990) 255.
[63] M.E. Casida, in: D.P. Chong (Ed.), Recent Advances in Density Functional Methods, vol. 1, World Scientific, Singapore, 1995, p. 155.
[64] E.U.K. Gross, J.F. Dobson, M. Petersilka, in: R.F. Nalewajski (Ed.), Springer Series 'Topics in Current Chemistry', vol., Springer, Heidelberg, 1996, p.
[65] E.K.U. Gross, C.A. Ullrich, U.J. Gossmann, vol. 337 of NATO ASI Ser. B, Plenum, New York, 1995, p. 149.
[66] M. Petersilka, U.J. Gossmann, E.K.U. Gross, Phys. Rev. Lett. 76 (1996) 1212.
[67] M. Petersilka, E.K.U. Gross, Int. J. Quantum Chem. Symposia 30 (1996) 181.
[68] S.J.A. van Gisbergen, J.G. Snijders, E.J. Baerends, J. Chem. Phys. 103 (1995) 9347.
[69] S.M. Colwell, N.C. Handy, A.M. Lee, Phys. Rev. A 53 (1996) 1316.
[70] C. Jamorski, M.E. Casida, D.R. Salahub, J. Chem. Phys. 104 (1996) 5134.
[71] R. Bauernschmitt, R. Ahlrichs, Chem. Phys. Lett. 256 (1996) 454.
[72] S.J.A. van Gisbergen, J.G. Snijders, E.J. Baerends, Comp. Phys. Commun. 118 (1999) 119.
[73] S.J.A. van Gisbergen, J.G. Snijders, E.J. Baerends, Phys. Rev. Lett. 78 (1997) 3097.
[74] S.J.A. van Gisbergen, J.G. Snijders, E.J. Baerends, J. Chem. Phys. 109 (1998) 1064.
[75] R. van Leeuwen, E.J. Baerends, Phys. Rev. A 49 (1994) 2421.
[76] R. van Leeuwen, O.V. Gritsenko, E.J. Baerends, Z. Phys. D 33 (1995) 229.
[77] S.H. Vosko, L. Wilk, M. Nusair, Can. J. Phys. 58 (1980) 1200.

[78] S.J.A. van Gisbergen, F. Koostra, P.R.T. Schipper, O.V. Gritsenko, J.G. Snijders, E.J. Baerends, Phys. Rev. A 57 (1998) 2556.
[79] ADF 'STO basis set database available on line at http://tc.chem.vu.nl/SCM/Doc/atomicdatabase'.
[80] A.A. Jarzecki, P.M. Kozlowski, P. Pulay, B.-H. Ye, X.-Y. Li, Spectrochimica Acta Part A 53 (1997) 1195.
[81] D. Lamoen, M. Parrinello, Chem. Phys. Lett. 248 (1996) 309.
[82] N. Matsuzawa, M. Ata, D.A. Dixon, J. Phys. Chem. 99 (1995) 7698.
[83] D. Sundholm, Chem. Phys. Lett. 317 (2000) 392.
[84] P.M. Kozlowski, T.S. Rush, III, A.A. Jarzecki, M.Z. Zgierski, B. Chase, C. Piffat, B.-H. Ye, X.-Y. Li, P. Pulay, T.G. Spiro, J. Phys. Chem. A103 (1999) 1357.
[85] A. Rosa, G. Ricciardi, E.J. Baerends, unpublished results (2001).
[86] W. Jentzen, I. Turowska-Tyrk, W.R. Scheidt, J.A. Shelnutt, Inorg. Chem. 35 (1996) 3559.
[87] A. Rosa, E.J. Baerends, Inorg. Chem. 33 (1994) 584.
[88] G. Ricciardi, A. Rosa, I. Ciofini, A. Bencini, Inorg. Chem. 38 (1999) 1422 (and references therein).
[89] H. Kobayashi, J. Chem. Phys. 30 (1959) 1373, 1362.
[90] H. Kuhn, Fortschr. Chem. Org. Naturstoffe 17 (1959) 404.
[91] J. Jusélius, D. Sundholm, Phys. Chem. Chem. Phys. 2 (2000) 2145.
[92] J. Jusélius, D. Sundholm, J. Organomet. Chem. 65 (2000) 5233.
[93] L. Edwards, D.H. Dolphin, M. Gouterman, J. Mol. Spectrosc. 35 (1970) 90.
[94] G.D. Dorough, J.R. Miller, F.M. Huennekens, J. Am. Chem. Soc. 73 (1951) 4315.
[95] H. Sekino, H. Kobayashi, J. Chem. Phys. 86 (1987) 5045.
[96] J. Fitzgerald, W. Taylor, H. Owen, Synthesis (1991) 686.
[97] S.S. Dvornikov, V.N. Knyukshto, V.A. Kuzmitskii, A.M. Shulga, K.N. Solovyov, J. Lumin. 23 (1981) 373.
[98] A. Rosa, G. Ricciardi, E.J. Baerends, J. Phys. Chem. 105 (2001) 5242.
[99] N. Kobayashi, in: C.C. Leznoff, A.B.P. Lever (Eds.), Phthalocyanines: Properties and Applications, vol. I, VCH Publishers, New York, 1993, p. 107.
[100] A. Rosa, G. Ricciardi, E.J. Baerends, unpublished results (2001).
[101] A. Starukhin, A. Shulga, J. Waluk, Chem. Phys. Lett. 272 (1997) 405.
[102] M.P. Pileni, M. Gratzel, J. Phys. Chem. 84 (1980) 1822.
[103] J.D. Keegan, A.M. Stolzenberg, Y.-C. Lu, R.E. Linder, G. Barth, A. Moscowitz, E. Bunnenberg, C. Djerassi, J. Am. Chem. Soc. 104 (1982) 4305.
[104] G.W. Canters, G. Jansen, M. Noort, J.H. van der Waals, J. Phys. Chem. 80 (1976) 2253.